

Dissecting Transformers: A CLEAR Perspective Towards Green AI

Hemang Jain^{1*} Shailender Goyal^{1*} Divyansh Pandey^{1*} Karthik Vaidhyathan¹

¹IIT Hyderabad
*Equal contribution

Abstract

The rapid adoption of Large Language Models (LLMs) has raised significant environmental concerns. Unlike the one-time cost of training, LLM inference occurs continuously and dominates the AI energy footprint. Yet most sustainability studies report only coarse model-level metrics, treating energy efficiency as an afterthought rather than a primary objective. Addressing the limitation, we propose **Component-Level Energy Assessment via Repetitions (CLEAR)**¹, to overcome temporal mismatch between microsecond(μ s) scale component execution and millisecond(ms) scale monitoring of energy sensors. Using CLEAR, we evaluate 15 models spanning four architecture types, keeping component-wise energy variance below **9.5%** while capturing over **90%** of total energy as individual components. We present the first comprehensive, fine-grained energy analysis of Transformer components across key parameters such as batch size, attention heads, hidden dimension, KV cache, and attention variants. Our findings reveal that Attention consumes significantly more Energy per FLOP as compared to the entire model, indicating that FLOPs alone fail to capture true component-level energy cost. CLEAR enables reliable fine-grained energy measurements and provides a strong formal foundation for predictive modelling of energy consumption.

1 Introduction

Large language models (LLMs) (OpenAI et al., 2024; Grattafiori et al., 2024; Yang et al., 2025) have transformed natural language processing, but their environmental costs are increasingly concerning. ChatGPT-4o alone has been estimated to produce about 150,000 tons of CO₂e in 2025, equivalent to annual emissions of 30,000 gasoline powered cars or the carbon sequestration of a forest the size of city of Chicago (Jegham et al., 2025).

While training and finetuning of LLMs is a computationally heavy and energy intensive process, it occurs infrequently. Inference, by contrast, happens continuously at a massive scale, with Gemini, GPT and Claude models serving hundreds of millions of queries daily. Consequently, even small reductions in per-inference energy consumption can translate into substantial global energy savings, making inference a critical target for optimizing the energy efficiency of LLMs.

Current research focuses on model-level energy consumption with high-level comparisons across different systems (Alizadeh and Castor, 2024; Sánchez-Mompó et al., 2025a). Recent works (Tian et al., 2025) increasingly rely on large datasets and report cumulative energy consumption across entire evaluation workloads rather than per-instance measurements. Such aggregate reporting obscures the contribution of individual architectural components (e.g., Attention and MLP layers) to overall energy consumption. It also limits the understanding of how energy consumption scales with factors such as the number of tokens, batch size, hidden dimension size, and variations or optimizations of specific components. Fine-grained energy measurements are therefore necessary to enable targeted optimizations and support informed architectural design decisions.

In our work, we introduce CLEAR, a simple and adoptable three stage pipeline for fine-grained inference energy measurement of individual components in the Transformer architecture. Unlike prior works limited to model and dataset level reporting (Faiz et al., 2024; Jegham et al., 2025; Casaña et al., 2023), CLEAR decomposes the Transformer architecture into constituent components, such as Embedding layer, Normalization blocks, Attention, and feed-forward MLP and measures the energy consumed by each component. Our approach enables a systematic comparison of energy consumption patterns across model architectures,

¹Code: <https://anonymous.4open.science/r/CLEAR-D487>

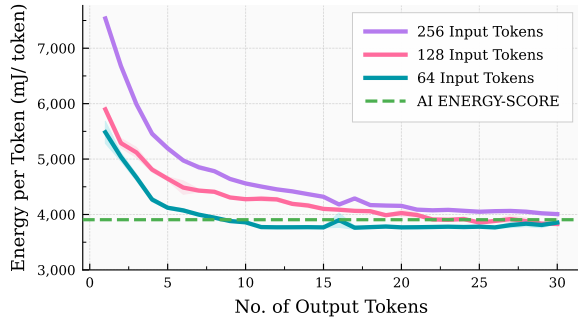


Figure 1: Comparison of the per-token energy reported by AI Energy Score (Luccioni and collaborators, 2025) with the fine-grained token-level measurements obtained using CLEAR. Aggregate benchmarks obscure variability in fine-grained, token-level energy usage.

components, Floating Point Operations (FLOPs), hidden dimensions, batch sizes, input and output token lengths, as well as different variants and optimization strategies.

A primary challenge arises from the temporal granularity mismatch between component execution and energy sensor monitoring as sub-operations complete within microseconds, whereas energy sensor provides power updates at tens of milliseconds. To address the gap, CLEAR employs an amplification strategy that stabilizes energy measurements. Another key challenge is the absence of a clear validation strategy for the reported energy measurements. CLEAR addresses the gap through a dedicated validation step based on two key metrics: (i) Completeness of the captured energy and (ii) Consistency across repeated trials. Our contributions are as follows :

- 1 We propose a three stage pipeline, CLEAR (Component-Level Energy Assessment via Repetitions) to overcome temporal mismatch between microsecond (μs) scale component execution and millisecond (ms) scale energy sensors. CLEAR is devised to measure energy consumption of fine-grained components in Transformer architecture.
- 2 Using CLEAR, we empirically analyse 15 models spanning four key Transformer architectures, measuring energy consumption of fine-grained components including Attention, MLP, LM Head, and Normalization blocks. We further isolate the impact of key factors such as FLOPs, number of tokens, hidden dimension size, number of attention heads, and batch size on energy consumption.
- 3 We conduct a controlled energy analysis to evaluate the impact of different Attention variants, optimization techniques, and KV Cache. Our findings reveal that energy consumed per FLOP varies

substantially across model components, with the Attention block exhibiting the highest energy consumption per FLOP among the components analyzed.

2 Related Works

Prior works to measure energy consumption of computationally small components falls mainly in two categories: (a) Methodologies that measure energy at a coarse granularity by measuring long sequences over large datasets and averaging to obtain per-token fine-grained approximations (Figure 1) (Cao et al., 2021; Schwartz et al., 2019). Tian et al. (2025) reports the energy values over large datasets at the scale of MJ which fails to reliably isolate the true fine-grained effect for different Attention variants. (b) Hardware-centric approaches that rely on execution tracing are tightly coupled with specific sensors or system instrumentation (Jegham et al., 2025; van der Vlugt et al., 2025; Alvi et al., 2021; Bridges et al., 2016). The additional sensor used needs to have low latency and high precision to reliably trace the function execution. Additionally, hardware based approaches are not scalable as they depend on specialized equipment and physical access to every target device making them difficult to deploy at scale. CLEAR departs from both paradigms by providing a component-level, software-based method validated for completeness and consistency. Operating entirely at application layer, CLEAR can be readily adopted across different hardware configurations and enables broader experimental space for energy analysis.

To improve accessibility, lightweight monitoring tools such as CodeCarbon and Carbontracker (Anthony et al., 2020) have emerged but, they still operate at a coarse granularity (a). More fine-grained approaches like FECOM (Rajput et al., 2024) and EDGEPROFILER (Pinnock et al., 2025), are targeted towards Tensorflow APIs and edge deployments respectively.

Recent works like Özcan et al. (2025) uses GPU-based simulations to study how batch size, sequence length, and parallelism influence inference efficiency. Extending real workloads, Fernandez et al. (2025) distinguish prefill and autoregressive stages, showing that optimizations can reduce energy consumption by up to 73%. Broader benchmarks, like *How Hungry is AI?* (Jegham et al., 2025), evaluate energy, water, and CO₂ footprints across hardware platforms, while the BLOOM case

study. Luccioni et al. (2023) was among the first to track emissions during the training and inference of a 176B parameter model. Luccioni and collaborators (2025) benchmarks over 160 models across multiple tasks, reporting GPU energy consumption in deep learning models. However, unlike prior works that report aggregate model-level energy consumption, CLEAR adopts a granular perspective, decomposing the Transformer architecture into its constituent components to analyze energy consumption across key axes.

3 Methodology

CLEAR uses a simple and easily adoptable, three-stage pipeline comprising the following stages: ① **Activation Store** to capture the sample activations, ② **Amplification Strategy** for reliable energy measurement and ③ **Validation** to verify the Completeness and Consistency of the energy analysis. CLEAR targets key computational primitives common to most transformer-based models. These include the **Attention** block that captures token-level dependencies, feed-forward **MLP** blocks for dense nonlinear transformations, **Normalization blocks** (Norm.), the **Embedding Layer** which maps discrete tokens into continuous vector spaces and the final **Language Modeling Head** (LM Head) that projects hidden representations back to the vocabulary space for output generation.

① Activation Store

The Activation Store \mathbf{A} serves as a cache of activations that allows isolated re-execution of individual components under identical input statistics, enabling fine-grained measurement of energy consumption. To enable component-wise energy profiling, we insert forward hooks at key points of the computation graph,

$$\mathcal{A} = \{\text{attn}, \text{mlp}, \text{lm_head}, \text{layer_norm} \dots\}$$

and capture the input activations at each hook. During a single forward pass, the hooks record for every component $c \in \mathcal{A}$ the corresponding activation tensor a_c for all tokens,

$$\mathbf{A} = \{a_c \mid c \in \mathcal{A}\}, \quad a_c \in \mathbb{R}^d.$$

② Amplification Strategy

Accurate energy measurement of Transformer components is challenging since the individual execution time is typically much shorter (μs) than the

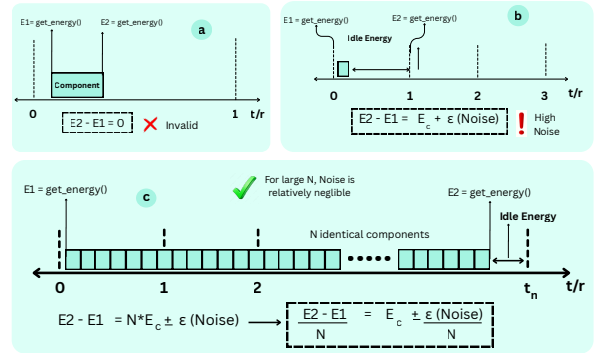


Figure 2: Comparison of Energy Sampling approaches. Case (c) demonstrates the sampling strategy followed by CLEAR to reduce the noise

sampling period of GPU power sensors. For example, NVIDIA’s NVML has a sensor read rate of about 20 to 50 ms. The temporal mismatch leads to two distinct sources of error (Refer Figure 2):

In case **a**, when the component completes execution within a few microseconds, entirely between two sensor samples, the monitoring sensor cannot update its reading in time due to which the observed energy is reported as zero:

$$E_2 - E_1 = 0, \quad (1)$$

even though the true component energy is non-zero. This leads to the energy consumption of smaller components being neglected and unaccounted.

In case **b**, if we supposedly measure energy after every sensor reading to capture the component’s energy consumption, the result remains highly noisy. This is because the measurement inevitably includes a significant amount of idle energy drawn by CUDA, making it hard to separate the true component energy. Consequently, when the execution only partially overlaps with a sensor’s sampling window, the observed energy is recorded as

$$E_2 - E_1 = E_c \pm \epsilon, \quad (2)$$

where E_c is the component’s actual energy consumed and ϵ represents noise.

To address above challenges, we adopt an amplification strategy, illustrated in **c** of Figure 2. As individual transformer components often complete the execution within 10–100 μs , their energy consumption remains highly noisy to NVML’s coarse sampling window. To obtain reliable readings, it is essential to minimize noise (ϵ) in the component energy measurement. This noise may arise from the model’s idle energy consumption or from inherent errors in the sensor measurements. To achieve this,

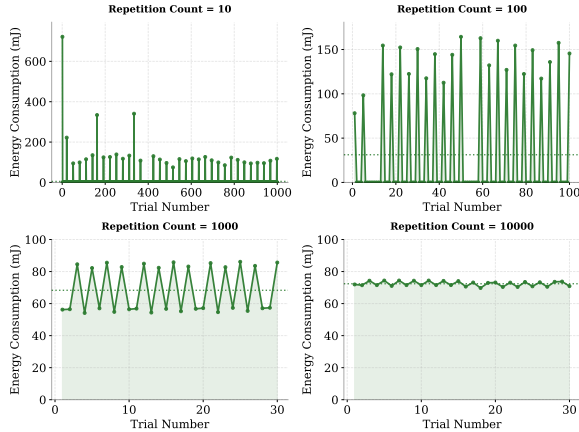


Figure 3: Effect of repeated sampling on energy measurements of the MLP block in Llama3.2-3B. As the repetition count increases, the variance in measured energy across trials decreases, indicating improved reliability of energy measurements.

each component is executed repeatedly in rapid succession on cached activations, without gaps between runs. This approach scales the effective runtime so that the total energy of the repeated executions dominates the idle background consumption, rendering the noise comparatively negligible.

Concretely, for each component c with cached input a_c , we measure the energy before and after N consecutive executions:

$$E_c^{\text{tot}} = \text{MeasureEnergy} \left(\sum_{i=1}^N c(a_c) \right). \quad (3)$$

The per-execution energy can then be obtained by averaging the total measured energy:

$$\hat{E}_c = \frac{E_{\text{end}} - E_{\text{start}}}{N} = \frac{E_c^{\text{tot}}}{N} \pm \frac{\varepsilon}{N}, \quad (4)$$

where ε denotes the measurement noise. By increasing N , the duration of the aggregated workload extends to hundreds of milliseconds such that execution time is larger than reading frequency of NVML’s power sensor while the noise term ε/N diminishes proportionally, yielding significantly reliable per-component energy measurements (Arafa et al., 2020) as shown in [c](#). We repeat the amplified measurement for T trials with a brief pause between runs to let the sensor reset, taking Average and Standard Deviation across trials to further smooth out sensor noise and make the per-component energy measurement more reliable.

3 Validation

Due to the lack of fine-grained energy analyses of individual components within Transformer architectures, the validation step in CLEAR verifies the

reliability of the measured energy along two key axes: (1) Consistency across repeated trials and (2) Completeness of the captured energy.

$$\text{StdDev}(\bar{E}_c) \rightarrow 0, \quad \bar{E}_{\text{model}} \approx \sum_{c \in \mathcal{C}} \bar{E}_c.$$

- i A standard deviation close to 0 indicates that repeated component-level energy measurements remain consistent across trials demonstrating high precision in energy measurements by CLEAR.
- ii The near-equality between the total measured model energy and sum of its per-component energies demonstrates that CLEAR is able to capture the component’s energy usage in a comprehensive manner.

4 Experimental Details

4.1 Hyperparameter & Hardware

As part of our experimental protocol, we evaluate two floating-point precisions, FP32 and FP16, while varying the input sequence length across 8, 32, 64, 128, 256 and 512 tokens to study the scaling effects. Each configuration is run for a fixed set of 20 trials ($T = 20$) to capture variability and validate precision. We assume FP16 precision unless explicitly stated.

We also investigate the effect of the repetition count N on reliability of the energy readings. As seen in Fig. 3, increasing repetition count (N) yields more stable readings and reduces measurement failures i.e. cases where the recorded energy for a trial is spuriously 0 mJ due to sensor granularity. Based on the analysis, we set the repetition count $N = 10,000$ for measurements of small components with execution time of order $100 \mu\text{s}$ and $N = 1,000$ for energy measurements of the full model, balancing measurement accuracy with computational cost.

Experiments were conducted on NVIDIA Ada-Lovelace GPUs (RTX 6000 Ada (NVIDIA, 2023)). The NVML interface typically updates power readouts only every 20–50 ms (Yang et al., 2024b; Nik et al., 2025) and introduced limitations in resolving microsecond-scale component execution, thereby requiring CLEAR for fine-grained energy attribution. Refer Appendix C for details.

4.2 Metrics

The energy consumed by each model component is measured in milliJoules(mJ), matching the $\approx 0.8\text{mJ}$ precision of the NVML sensor used. For validating

Component	8 Tokens		32 Tokens		64 Tokens		96 Tokens		128 Tokens	
	Avg.	Std. Dev.	Avg.	Std. Dev.	Avg.	Std. Dev.	Avg.	Std. Dev.	Avg.	Std. Dev.
Attention Block	53.261	1.677	64.147	0.686	75.161	0.76	93.91	0.779	100.701	1.045
MLP	685.408	12.61	776.905	3.166	867.687	0.867	958.134	1.406	1046.2	1.187
Norm. (All)	9.324	0.729	10.787	0.825	12.702	1.056	13.443	1.422	14.639	1.108
Captured (Block)	747.993	-	851.839	-	955.55	-	1065.487	-	1161.541	-
Block	731.905	12.456	856.309	1.428	951.869	0.805	1057.01	0.881	1157.197	1.181
% Capture (Block)	102.198	-	99.478	-	100.387	-	100.802	-	100.375	-
Embedding Layer	0.568	0.215	0.627	0.282	1.061	0.41	1.077	0.434	0.766	0.357
LM Head	443.391	1.108	452.139	0.988	460.383	0.988	475.22	1.265	483.515	1.242
Final Layer Norm.	4.695	0.368	5.14	0.361	6.071	0.496	6.625	0.525	7.221	0.466
Captured (Model)	18014.38	-	21009.32	-	23312.36	-	25851.15	-	28264.24	-
Model	18447.5	63.784	21366.69	103.479	24126.47	12.67	26634.05	15.33	28801.98	2.867
% Capture (Model)	97.652	-	98.327	-	96.626	-	97.061	-	98.133	-

Table 1: Energy Consumption for GPT-OSS-20B model across different input token length with %Capture (96+%) for Block and Full Model and Std. Deviation of Energy Consumed across 20 trials. All energy units in mJ.

our methodology (ii), we define two complementary metrics, **Energy Captured** (Capture) and **Percentage Capture** (%Capture). Energy Captured (in mJ) represents the total energy measured across all the major components of a given layer block or the entire model. Due to the limited precision of the instrumentation, we neglect negligible contributors (e.g., residual connections) and introduce %Capture to indicate how well CLEAR accounts for the model’s overall energy usage. Specifically, %Capture is the ratio of the measured Energy Captured to the model’s measured energy consumption, expressed as a percentage:

$$\text{Capture} = \sum_{i=1}^N \bar{E}_i, \quad \% \text{Capture} = \frac{\sum_{i=1}^N \bar{E}_i}{\bar{E}_{\text{model}}} \times 100$$

CLEAR quantifies the computation executed by each component using FLOPs and measures GPU execution time (μs) using the PyTorch Profiler. To evaluate the energy cost per unit of computation, we define two metrics:

$$\text{E/FLOP} = \frac{\text{Energy [mJ]}}{\text{FLOPs} \times 10^{-9}}$$

$$\Delta E / \Delta \text{FLOP} = \frac{\Delta \text{Energy [mJ]}}{\Delta \text{FLOPs} \times 10^{-9}}.$$

The metric E/FLOP (expressed in mJ/GFLOP), represents the average energy cost per unit computation, where lower values indicate higher energy efficiency. The marginal metric $\Delta E / \Delta \text{FLOP}$ measures the additional energy consumed per extra GFLOP, capturing the sensitivity of energy consumption to increased computational demand.

For details about list of models and transformer architectures, Refer Appendices A and B

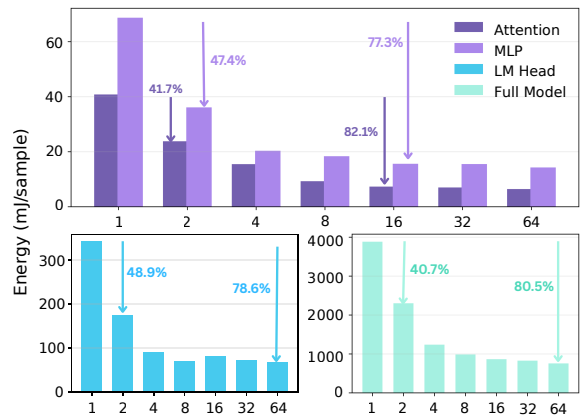


Figure 4: Energy consumed per sample by different components of Llama-3.2-3B as a function of batch size. Increasing the batch size significantly improves energy efficiency. X-axis represents the Batch size.

5 Results

Completeness of Energy Captured: Despite the omission of very small and negligible components, the overall %Capture at both the block and model level consistently remains above 90% across different models (Refer Table 1 and Appendix G). As per (ii), we observe that energy of individual components provide a reliable and near-complete estimate of the total energy consumption dictated by the model’s architecture. However we consistently observe low %Capture(Block) of ALBERT variants possible due to factorized embeddings causing higher idle energy consumption.

Consistency Across Trials : Using CLEAR, we observe that the average standard deviation of the measured component energies consistently remains below 9.5% of the respective mean for components consuming $> 5\text{mJ}$ of energy. As component size

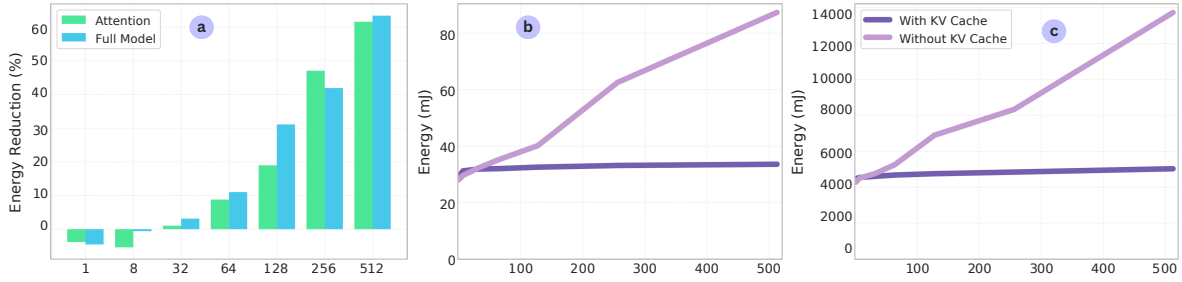


Figure 5: (a) Percentage reduction in energy due to KV cache for Attention and full model across different input sequence lengths. (b) and (c) show the energy consumption of the Attention block and full model, respectively, as a function of input token length during single-token generation. Experiments are performed on Qwen2.5-3B.

and execution time increase, the relative standard deviation decreases (eg: components consuming approximately 1J show deviations as low as 1% ⁱ). Such behavior arises because shorter executions yield fewer sensor samples, making measurements more sensitive to idle-energy noise and the sensor’s precision limits (Refer Appendix D.)

5.1 Batch Size

Empirically, we observe that increasing the batch size leads to a substantial reduction in per-sample energy consumption. **CLEAR** investigates the effect of individual model components in overall energy savings. Even a modest increase to a batch size of 2 results in a significant reduction of approximately 40–45% (See Figure 4) in per-sample energy across major components. The reduction is slightly more pronounced in the MLP blocks compared to the Attention blocks due to higher arithmetic intensity and more efficient utilization of GPU compute units. At larger batch sizes, the per-sample energy consumption decreases by up to 80%. These results indicate that batching is a critical optimization not only at the system level but also within the internal components of the model.

5.2 Impact of KV Cache

Using **CLEAR**, we extend the analysis beyond single-token *Prefill* stage to study realistic multi-token generation in Decoder-only Transformer models. In autoregressive *Decode* stage, each generated token attends to all previously processed tokens. Without optimization, decoding requires recomputing the Key (K) and Value (V) projections for the entire sequence at every generation step, leading to substantial increase in computational cost and energy consumption as the sequence length grows. Key–Value (KV) cache eliminates the computational redundancy by storing previously computed K and V tensors during the *Prefill* stage and reusing them during subsequent *Decode*

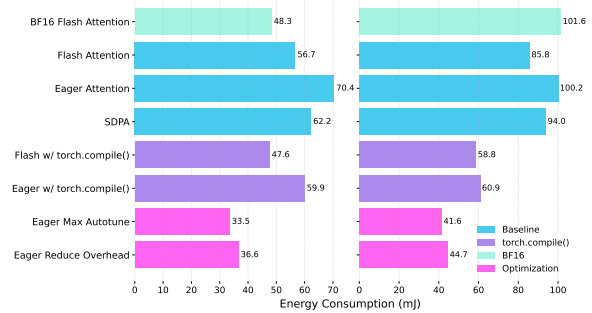


Figure 6: Energy Consumption for different variants and optimizations of Attention Mechanism on Qwen2.5-3B (left) and Gemma3-4B (right) on 256 input tokens

steps. During decoding, only the Query (Q) for the newly generated token must be computed, while all previous keys and values are retrieved directly from the cache, reducing both computation and memory movement. (Refer Appendix E for more details)

Empirically, we observe that KV Cache has a substantial impact on energy efficiency. When KV cache is enabled, both the FLOPs (~ 0.019 GFLOPs) and energy consumption of the attention mechanism remain nearly constant across increasing sequence lengths. In contrast, disabling KV cache results in rapid increase of computational cost, with FLOPs rising to 9.667 GFLOPs and energy increasing from 28.05 mJ to 87.36 mJ as the input sequence grows from 1 to 512 tokens (See Figure 5 ^b). As seen in ^a, KV cache reduces Energy consumption by more than 60% at longer contexts whereas the energy gains are negligible for shorter sequences of about 50 input tokens.

5.3 Attention Variants & Optimizations

CLEAR, with its Amplification Strategy, enables fine-grained energy analysis of different component variants and optimizations. We compare three Attention implementations: *Eager Attention*, *Scaled Dot-Product Attention (SDPA)*, and *Flash Attention*. Across both models, Flash Attention consistently consumes less energy than Eager At-

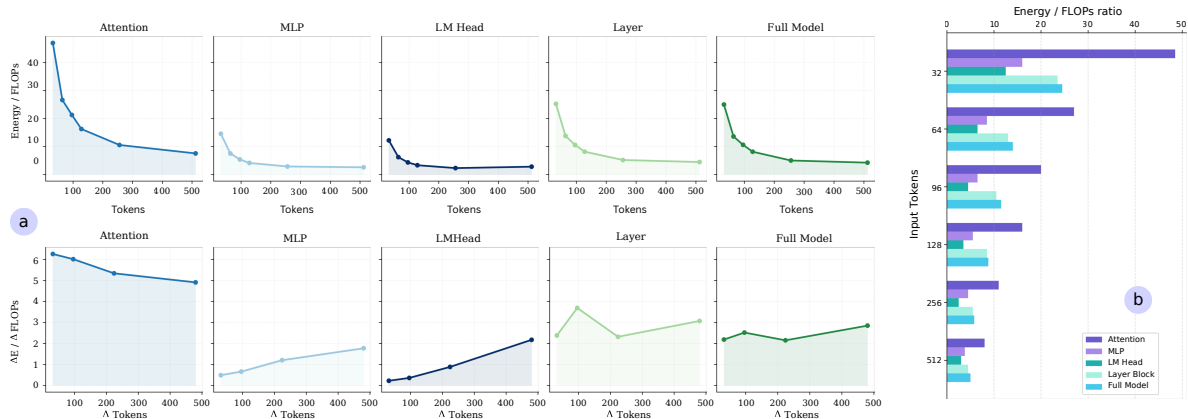


Figure 7: (a) Variation of E/FLOP and $\Delta E/\Delta \text{FLOP}$ for Gemma3-4B model across major components. E/FLOP ratio decreases with input sequence length, while marginal energy consumed per FLOP remains nearly constant. (b) Attention consistently shows the highest E/FLOP ratio across all input lengths.

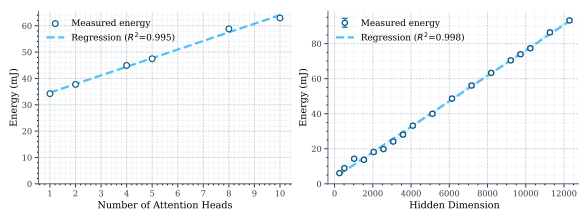


Figure 8: Energy Scaling for Attention and MLP block as a function of Number of Attention Heads (left) and Hidden Dimension (right) respectively.

attention, while SDPA falls in between. This occurs because Eager Attention materializes the full attention matrix, increasing memory traffic and kernel launches whereas Flash Attention computes attention in tiled blocks without storing the complete matrix, reducing memory movement, and improving energy efficiency (Refer Figure 6)

Applying `torch.compile()` further reduces energy consumption for both Flash and Eager implementations. The improvement comes from graph-level optimizations that fuse multiple small kernels into larger kernels, reducing kernel launch overhead and improving GPU utilization. Refer Appendix F for more details about the optimizations. The largest reduction in energy is observed with the **Max Autotune** and **Reduced Overhead** optimizations, as they aggressively fuse operations and remove runtime overheads such as profiling and synchronization, resulting in more efficient execution paths with fewer intermediate operations.

5.4 Hidden Dimension & Attention Heads

As shown in Figure 8, we observe that Energy Consumed by the MLP block scales almost perfectly linearly with the hidden dimension size, with only a very small constant overhead (approximately 0.7 mJ per 100 hidden dimensions). The

behavior is expected because the MLP is primarily composed of dense matrix multiplications whose computational cost increases proportionally with the hidden dimension. In contrast, the Attention block exhibits a substantially larger constant overhead. For a configuration with 256 hidden dimensions, the constant energy cost is approximately 31.34 mJ, and the energy consumption increases by about 3.27 mJ per additional Attention Head.

Above observations have important architectural implications. Increasing the hidden dimension mainly affects the MLP energy cost and scales in a predictable linear manner. In contrast, increasing the number of attention heads introduces both a significant baseline cost and an additional per-head overhead, making attention scaling relatively more energy expensive.

5.5 FLOPs & Energy

As shown in Figure 7 (b), across all input token lengths, the Attention mechanism consistently exhibits a higher Energy/FLOP ratio than MLP layers, LM-Head and overall model. MLP and LM-Head layers consist dense matrix multiplications and are efficiently accelerated by GPUs, executing more computations per unit of energy. Attention, however, involves multiple stages like query-key dot product, softmax operations, and irregular memory accesses that can introduce additional memory and synchronization overheads.

As shown in figure 7 (a), we consistently observe that E/FLOP ratio decreases as the input sequence length increases for all components. When longer sequences are processed, the fixed costs associated with computation are amortized over a larger number of tokens. To better isolate the energy

associated with additional computation, we analyze the marginal energy cost per FLOP, defined as $\Delta E/\Delta \text{FLOP}$. The marginal energy remains approximately constant as input length increases across model components indicating a strong empirical evidence that FLOPs are the primary driver of the **variable** portion of energy consumption and can be decomposed as

$$E(L) \approx E_0 + k \cdot \text{FLOPs}(L) \quad (5)$$

where E_0 denotes a fixed energy overhead and k represents the marginal energy cost per FLOP. L denotes input length and only the second term grows nearly linearly with the computational workload (FLOPs). k is component-dependent constant of proportionality and is noticeably higher for the Attention mechanism. Overall results indicate that while FLOPs explain the variable component of energy consumption, accurate component-level energy estimation must account for fixed overheads (E_0) and component-specific marginal costs (k).

6 Discussion

Most sustainability studies have primarily focused on model-level energy consumption, treating LLMs as *monoliths* and paying little attention to the heterogeneity of their internal components from a sustainability perspective. **CLEAR**'s contribution to measure energy consumption at component-level granularity has direct implications for the research community as it provides a systematic methodology to reliably measure internal energy dynamics and enable targeted energy optimizations at the design level of model architecture.

Previous works (Cao et al., 2021; Yang et al., 2024c; van der Vlugt et al., 2025; S et al., 2024) do measure energy consumption using the two paradigms: **a** Using large datasets and model-level granularity **b** Hardware-based approach. However, the above works explicitly acknowledge a key limitation: the coarse sampling frequency of available GPU/CPU energy sensors fundamentally restricts the granularity at which Energy consumption can be attributed at the software scale. As a result, they are unable to isolate the actual energy usage of microsecond-scale sub-operations or validate whether the reported estimates precisely reflect true energy consumption. **CLEAR**'s three-stage pipeline is hardware agnostic as it runs at an application/software level which allows easy adapt-

ability for fine-grained energy analysis in Transformer architectures.

As discussed in Section 5.5, we observe that each component consumes energy disproportionately, posing a threat to use FLOPs and related metrics as convenient proxies for energy consumption (Getzner et al., 2023; Özcan et al., 2025) as component-level disparities are systematically obscured by model-level aggregate measurements.

As seen in Section 5, **CLEAR** demonstrates statistically reliable and sufficiently complete component-wise energy profiling that can be employed to support comparative energy analysis and draw robust conclusions about energy implications of specific design choices. **CLEAR** establishes a foundation for future work on predictive modeling so that the energy costs can be computed based on architectural design choices like hidden dimensions, number of layers, etc., allowing accurate, generalizable prediction of component-wise energy in the early design stages. This aligns with the growing emphasis on Green AI and the need for energy-aware, sustainable AI system design. (Bolón-Canedo et al., 2024; Sánchez-Mompó et al., 2025b; Różycki et al., 2025)

CLEAR provides a strong formal foundation for predictive modeling of energy consumption and enables the recording of reliable and accurate ground-truth measurements. Previous works like IrEne (Cao et al., 2021) use a regression-based prediction model on feature dimensions to predict the energy consumption of the model. **CLEAR** can enhance IrEne's energy prediction approach by providing large-scale, reliable ground truths and insights on the impact of different parameters on energy for better predictive modeling.

7 Conclusion

Taken together, **CLEAR**'s findings underscore that sustainability in AI must be treated as **a first-class research objective rather than an afterthought**. By moving beyond aggregate model-level reporting to examine component-level dynamics, we aim to motivate the software and AI research communities to pursue progress that is both holistic and environmentally responsible, driven by a proactive rather than reactive mindset. Looking forward, we hope this work inspires future research to integrate energy considerations into every stage of model development, fostering AI systems that are not only performant but also sustainable.

8 Limitations

While our study provides the first component-level view of energy consumption in Transformer architectures, a few aspects merit further exploration.

First, our energy estimates rely on NVIDIA's NVML interface and FLOP counts obtained via the PyTorch Profiler. Though there are well-established tools, but like all measurement frameworks they may carry some inherent uncertainties that may slightly affect the results by negligible margin.

Second, GPU hardware introduces additional variability. Different GPU families and generations apply their own low-level optimization, potentially affecting the energy profiles of specific computational components. Extending this analysis across a wider range of hardware would sharpen our understanding of how these optimizations influence component-wise energy usage. While it is left for future work, to the best of our knowledge, our study remains the first systematic investigation of component-level energy dynamics in Transformer models, providing a foundational understanding of the challenges and opportunities present on current hardware.

Finally, because prior literature offers little precedent for fine-grained energy measurement of individual Transformer components, our validation protocol represents an initial step. Future work can strengthen and expand these validation methods as the research community develops more sophisticated benchmarks and measurement standards.

Ethical Considerations

This work studies the energy consumption of Transformer-based models at a fine-grained component level to better understand and improve the environmental efficiency of large language model inference. The proposed **CLEAR** framework measures energy consumption of internal model components under controlled experimental conditions using publicly available models and standard hardware instrumentation.

Our work does not involve human subjects, personal data, or sensitive information. While the methodology could be used to optimize systems for energy efficiency, we emphasize that such optimizations should be considered alongside other AI considerations such as safety, fairness, and reliability. Overall, our work aims to support the development of more sustainable and environmentally responsible AI systems.

References

- Marah Abdin, Jyoti Aneja, Harkirat Behl, Sébastien Bubeck, Ronen Eldan, Suriya Gunasekar, Michael Harrison, Russell J. Hewett, Mojan Javaheripi, Piero Kauffmann, James R. Lee, Yin Tat Lee, Yuanzhi Li, Weishung Liu, Caio C. T. Mendes, Anh Nguyen, Eric Price, Gustavo de Rosa, Olli Saarikivi, and 8 others. 2024. [Phi-4 technical report](#). *Preprint*, arXiv:2412.08905.
- AI@Meta. 2024. [Llama 3 model card](#).
- Negar Alizadeh and Fernando Castor. 2024. [Green ai: a preliminary empirical study on energy consumption in dl models across different runtime infrastructures](#). In *Proceedings of the IEEE/ACM 3rd International Conference on AI Engineering - Software Engineering for AI*, CAIN 2024, page 134–139. ACM.
- Hamza Mustafa Alvi, Hammad Majeed, Hasan Mujtaba, and Mirza Omer Beg. 2021. [Mlee: Method level energy estimation — a machine learning approach](#). *Sustainable Computing: Informatics and Systems*, 32:100594.
- Lasse F. Wolff Anthony, Benjamin Kanding, and Raghavendra Selvan. 2020. [Carbontracker: Tracking and predicting the carbon footprint of training deep learning models](#). *Preprint*, arXiv:2007.03051.
- Yehia Arafa, Ammar ElWazir, Abdelrahman ElKanishy, Youssef Aly, Ayatelrahman Elsayed, Abdel-Hameed Badawy, Gopinath Chennupati, Stephan Eidenbenz, and Nandakishore Santhi. 2020. [Verified instruction-level energy consumption measurement for nvidia gpus](#). In *Proceedings of the 17th ACM International Conference on Computing Frontiers*, CF '20, page 60–70. ACM.
- Verónica Bolón-Canedo, Laura Morán-Fernández, Brais Cancela, and Amparo Alonso-Betanzos. 2024. [A review of green artificial intelligence: Towards a more sustainable future](#). *Neurocomput.*, 599(C).
- Robert A. Bridges, Neena Imam, and Tiffany M. Mintz. 2016. [Understanding gpu power: A survey of profiling, modeling, and simulation methods](#). *ACM Comput. Surv.*, 49(3).
- Qingqing Cao, Yash Kumar Lal, Harsh Trivedi, Aruna Balasubramanian, and Niranjana Balasubramanian. 2021. [Irene: Interpretable energy prediction for transformers](#). *Preprint*, arXiv:2106.01199.
- Joel Castaño, Silverio Martínez-Fernández, Xavier Franch, and Justus Bogner. 2023. [Exploring the carbon footprint of hugging face's ml models: A repository mining study](#). In *2023 ACM/IEEE International Symposium on Empirical Software Engineering and Measurement (ESEM)*, page 1–12. IEEE.
- Hyung Won Chung, Le Hou, Shayne Longpre, Barret Zoph, Yi Tay, William Fedus, Yunxuan Li, Xuezhi Wang, Mostafa Dehghani, Siddhartha Brahma, Albert Webson, Shixiang Shane Gu, Zhuyun Dai, Mirac

- Suzgun, Xinyun Chen, Aakanksha Chowdhery, Alex Castro-Ros, Marie Pellat, Kevin Robinson, and 16 others. 2022. [Scaling instruction-finetuned language models](#). *Preprint*, arXiv:2210.11416.
- Jacob Devlin, Ming-Wei Chang, Kenton Lee, and Kristina Toutanova. 2019. [Bert: Pre-training of deep bidirectional transformers for language understanding](#). *Preprint*, arXiv:1810.04805.
- Ahmad Faiz, Sotaro Kaneda, Ruhan Wang, Rita Osi, Prateek Sharma, Fan Chen, and Lei Jiang. 2024. [Llm-carbon: Modeling the end-to-end carbon footprint of large language models](#). *Preprint*, arXiv:2309.14393.
- Jared Fernandez, Clara Na, Vashisth Tiwari, Yonatan Bisk, Sasha Luccioni, and Emma Strubell. 2025. [Energy considerations of large language model inference and efficiency optimizations](#). *Preprint*, arXiv:2504.17674.
- Johannes Getzner, Bertrand Charpentier, and Stephan Günnemann. 2023. [Accuracy is not the only metric that matters: Estimating the energy consumption of deep learning models](#). *Preprint*, arXiv:2304.00897.
- Aaron Grattafiori, Abhimanyu Dubey, Abhinav Jauhri, Abhinav Pandey, Abhishek Kadian, Ahmad Al-Dahle, Aiesha Letman, Akhil Mathur, Alan Schelten, Alex Vaughan, Amy Yang, Angela Fan, Anirudh Goyal, Anthony Hartshorn, Aobo Yang, Archi Mitra, Archie Sravankumar, Artem Korenev, Arthur Hinsvark, and 542 others. 2024. [The llama 3 herd of models](#). *Preprint*, arXiv:2407.21783.
- Nidhal Jegham, Marwan Abdelatti, Lassad Elmoubarki, and Abdeltawab Hendawi. 2025. [How hungry is ai? benchmarking energy, water, and carbon footprint of llm inference](#). *Preprint*, arXiv:2505.09598.
- Zhenzhong Lan, Mingda Chen, Sebastian Goodman, Kevin Gimpel, Piyush Sharma, and Radu Soricut. 2020. [Albert: A lite bert for self-supervised learning of language representations](#). *Preprint*, arXiv:1909.11942.
- Mike Lewis, Yinhan Liu, Naman Goyal, Marjan Ghazvininejad, Abdelrahman Mohamed, Omer Levy, Veselin Stoyanov, and Luke Zettlemoyer. 2019. [BART: denoising sequence-to-sequence pre-training for natural language generation, translation, and comprehension](#). *CoRR*, abs/1910.13461.
- Yinhan Liu, Myle Ott, Naman Goyal, Jingfei Du, Mandar Joshi, Danqi Chen, Omer Levy, Mike Lewis, Luke Zettlemoyer, and Veselin Stoyanov. 2019. [Roberta: A robustly optimized bert pretraining approach](#). *Preprint*, arXiv:1907.11692.
- Alexandra Sasha Luccioni, Sylvain Viguier, and Anne-Laure Ligozat. 2023. [Estimating the carbon footprint of bloom, a 176b parameter language model](#). *Journal of Machine Learning Research*, 24(253):1–15.
- Sasha Luccioni and collaborators. 2025. [Announcing AI Energy Score Ratings](#). Accessed: 2025-09-06.
- Alireza Nik, Michael A. Riegler, and Pål Halvorsen. 2025. [Energy-conscious llm decoding: Impact of text generation strategies on gpu energy consumption](#). *Preprint*, arXiv:2502.11723.
- NVIDIA. 2023. [Nvidia rtx 6000 ada generation datasheet](#). Technical Datasheet (PDF). Official specifications for the RTX 6000 Ada, including CUDA/RT/Tensor cores, memory, bandwidth, and power.
- OpenAI. 2025. [gpt-oss-120b & gpt-oss-20b model card](#). *Preprint*, arXiv:2508.10925.
- OpenAI, Josh Achiam, Steven Adler, Sandhini Agarwal, Lama Ahmad, Ilge Akkaya, Florencia Leoni Aleman, Diogo Almeida, Janko Altenschmidt, Sam Altman, Shyamal Anadkat, Red Avila, Igor Babuschkin, Suchir Balaji, Valerie Balcom, Paul Baltescu, Haiming Bao, Mohammad Bavarian, Jeff Belgum, and 262 others. 2024. [Gpt-4 technical report](#). *Preprint*, arXiv:2303.08774.
- Alyssa Pinnock, Shakya Jayakody, Kawsher A Roxy, and Md Rubel Ahmed. 2025. [Edgeprofiler: A fast profiling framework for lightweight llms on edge using analytical model](#). *Preprint*, arXiv:2506.09061.
- PNY. 2023. [Nvidia rtx 5000 ada generation datasheet](#). Product Datasheet (PDF). Specifications include CUDA cores, Tensor/RT cores, memory capacity, bandwidth, and board power.
- Saurabhsingh Rajput, Tim Widmayer, Ziyuan Shang, Maria Kechagia, Federica Sarro, and Tushar Sharma. 2024. [Enhancing energy-awareness in deep learning through fine-grained energy measurement](#). *Preprint*, arXiv:2308.12264.
- Rafał Różycki, Dorota Agnieszka Solarska, and Grzegorz Waligóra. 2025. [Energy-aware machine learning models—a review of recent techniques and perspectives](#). *Energies*, 18(11).
- Shivadharshan S, Akilesh P, Rajrupa Chattaraj, and Sridhar Chimalakonda. 2024. [Cp joules: An energy measurement tool for c++](#). *Preprint*, arXiv:2412.13555.
- Victor Sanh, Lysandre Debut, Julien Chaumond, and Thomas Wolf. 2020. [Distilbert, a distilled version of bert: smaller, faster, cheaper and lighter](#). *Preprint*, arXiv:1910.01108.
- Roy Schwartz, Jesse Dodge, Noah A. Smith, and Oren Etzioni. 2019. [Green ai](#). *Preprint*, arXiv:1907.10597.
- Adrián Sánchez-Mompó, Ioannis Mavromatis, Peizheng Li, Konstantinos Katsaros, and Aftab Khan. 2025a. [Green mlops to green genops: An empirical study of energy consumption in discriminative and generative ai operations](#). *Information*, 16(4):281.
- Adrián Sánchez-Mompó, Ioannis Mavromatis, Peizheng Li, Konstantinos Katsaros, and Aftab Khan. 2025b. [Green mlops to green genops: An empirical study of](#)

energy consumption in discriminative and generative ai operations. *Information*, 16(4).

Gemma Team. 2024. [Gemma: Open models based on gemini research and technology](#). *Preprint*, arXiv:2403.08295.

Zhengyu Tian, Anantha Padmanaban Krishna Kumar, Hemant Krishnakumar, and Reza Rawassizadeh. 2025. [Attentions under the microscope: A comparative study of resource utilization for variants of self-attention](#). *Preprint*, arXiv:2507.07247.

Steven van der Vlugt, Leon Oostrum, Gijs Schoonderbeek, Ben van Werkhoven, Bram Veenboer, Krijn Doekemeijer, and John W. Romein. 2025. [Powersensor3: A fast and accurate open source power measurement tool](#). *Preprint*, arXiv:2504.17883.

Ashish Vaswani, Noam Shazeer, Niki Parmar, Jakob Uszkoreit, Llion Jones, Aidan N. Gomez, Lukasz Kaiser, and Illia Polosukhin. 2023. [Attention is all you need](#). *Preprint*, arXiv:1706.03762.

An Yang, Anfeng Li, Baosong Yang, Beichen Zhang, Binyuan Hui, Bo Zheng, Bowen Yu, Chang Gao, Chengen Huang, Chenxu Lv, Chujie Zheng, Dayiheng Liu, Fan Zhou, Fei Huang, Feng Hu, Hao Ge, Haoran Wei, Huan Lin, Jialong Tang, and 41 others. 2025. [Qwen3 technical report](#). *Preprint*, arXiv:2505.09388.

An Yang, Baosong Yang, Binyuan Hui, Bo Zheng, Bowen Yu, Chang Zhou, Chengpeng Li, Chengyuan Li, Dayiheng Liu, Fei Huang, Guanting Dong, Haoran Wei, Huan Lin, Jialong Tang, Jialin Wang, Jian Yang, Jianhong Tu, Jianwei Zhang, Jianxin Ma, and 43 others. 2024a. [Qwen2 technical report](#). *Preprint*, arXiv:2407.10671.

Zeyu Yang, Karel Adamek, and Wesley Armour. 2024b. [Accurate and convenient energy measurements for gpu: A detailed study of nvidia gpu’s built-in power sensor](#). In *SC24: International Conference for High Performance Computing, Networking, Storage and Analysis*, page 1–17. IEEE.

Zeyu Yang, Karel Adamek, and Wesley Armour. 2024c. [Accurate and convenient energy measurements for gpu: A detailed study of nvidia gpu’s built-in power sensor](#). In *SC24: International Conference for High Performance Computing, Networking, Storage and Analysis*, pages 1–17.

Miray Özcan, Philipp Wiesner, Philipp Weiß, and Odej Kao. 2025. [Quantifying the energy consumption and carbon emissions of llm inference via simulations](#). *Preprint*, arXiv:2507.11417.

A Models

To conduct a systematic study of energy consumption across architectural paradigms, we consider four representative classes of Transformer-based models namely **Encoder-only** models, **Decoder-only** models, **Encoder-Decoder** models and sparse-activated **Mixture of Experts** (MOE) variants. Our model selection aims to balance breadth of architectural diversity with controlled comparisons of scale and design choices.

We evaluate eight widely-used Encoder only models namely BERT-base, BERT-large (Devlin et al., 2019), ALBERT-base, ALBERT-large (Lan et al., 2020), RoBERTa-base, RoBERTa-large (Liu et al., 2019) and distilled variants DistilBERT and DistilBERT (Sanh et al., 2020). Base and large versions allow us to isolate the effect of model size on energy usage where distilled counterparts enable comparison with lightweight compression techniques. To represent contemporary LLMs i.e. Decoder-only models, we experiment with instruction-tuned variants of four key open-source families namely LLaMA 3.2-3B (AI@Meta, 2024), Gemma 3-4B (Team, 2024), Qwen 2.5-3B (Yang et al., 2024a), and Phi-4-4B (Abdin et al., 2024). We focus specifically on single-token generation to control for variability in output sequence length and to minimize cache based auto-regressive generation. We also evaluate **CLEAR** on two well-established sequence-to-sequence models, namely BART (Lewis et al., 2019) and FLAN-T5 (Chung et al., 2022) and a sparse-activated MoE, GPT-OSS-20B (OpenAI, 2025)

B Transformer Architectures

Despite architectural differences, the transformer based models share a set of common computational primitives. The detailed flow of how the model produces its output is illustrated in the following.

Let \mathcal{V} denote the vocabulary space, and $x = (x_1, \dots, x_T)$, $x_t \in \mathcal{V}$ be an input token sequence of length T . A tokenizer $\mathcal{T} : \mathcal{V} \rightarrow \{1, \dots, |\mathcal{V}|\}$ maps tokens to discrete indices. The indices are embedded into a continuous space by the **Embedding Layer** $E \in \mathbb{R}^{|\mathcal{V}| \times d}$:

$$h_t^0 = E[x_t] + P_t, \quad t = 1, \dots, T,$$

where $P_t \in \mathbb{R}^d$ denotes the positional embedding and d is the hidden dimensionality. Embeddings are then passed to a set of Transformer layers each consisting of an **Attention** (Attn) block

followed by a position-wise Feed-Forward **MLP** block, interleaved with residual connections and **Normalization** blocks for numerical stability, as depicted in the Transformer block of Figure 2. For layer $\ell \in \{1, \dots, L\}$, the computations are:

$$\begin{aligned}\tilde{h}^\ell &= \text{LN}(h^{\ell-1}), \quad z^\ell = h^{\ell-1} + \text{Attn}(\tilde{h}^\ell) \\ h^\ell &= z^\ell + \text{FFN}(\text{LN}(z^\ell)).\end{aligned}$$

However, the placement of Normalization blocks vary across different models and can be applied at different stages within a layer block. Post all layers, the final hidden state $h^L \in \mathbb{R}^{T \times d}$ is projected onto the vocabulary using the language modeling head:

$$\hat{y}_t = \text{softmax}(h_t^L W_{\text{LM}}^\top), \quad W_{\text{LM}} \in \mathbb{R}^{|\mathcal{V}| \times d}.$$

B.1 Encoder-Only

Encoder-only architectures (e.g., BERT, RoBERTa, ALBERT) compute contextualized token representations using bidirectional self-attention. They are commonly used for classification, token-level prediction and masked-language-modeling objectives. The encoder processes the full input x in parallel, producing $H^L = (h_1^L, \dots, h_T^L) \in \mathbb{R}^{T \times d}$ which can be pooled or projected to task heads.

Encoder-only architectures typically use a *dense attention pattern*, meaning that no causal mask is applied to restrict attention. Formally, the attention operation is defined as

$$\text{Attn}(Q, K, V) = \text{softmax}\left(\frac{QK^\top}{\sqrt{d_k}}\right)V, \quad (6)$$

where every token can attend to every other token in the sequence. This design produces *symmetric contextualization*, since information can flow bidirectionally across tokens. However, it comes with a computational cost of $\mathcal{O}(T^2d)$ per layer (due to the pairwise interactions between all tokens) and a memory cost of $\mathcal{O}(T^2)$ for storing the attention weights.

Different tasks attach specialized output heads on top of the final hidden states $h_t^L \in \mathbb{R}^d$. For **token-level classification**, each token representation is projected into the label space using a weight matrix W_{tok} . The predicted class distribution for token t is given by

$$\hat{y}_t = \text{softmax}\left(h_t^L W_{\text{tok}}^\top\right).$$

For **sequence-level classification**, the hidden state of a special token such as [CLS] serves as a

summary vector for the entire sequence. This representation h_{cls}^L is then passed through a classifier, typically implemented as a multi-layer perceptron (MLP):

$$h_{\text{cls}}^L \mapsto \text{MLP}(h_{\text{cls}}^L).$$

For **masked language modeling (MLM)**, the prediction head reuses the input embedding matrix E to tie input and output representations. In this case, the output weight matrix is defined as

$$W_{\text{LM}} = E.$$

This weight sharing enforces consistency between how tokens are encoded and how they are predicted.

Encoder-only designs maximize parallelizability during training as the whole sequence is processed concurrently, but the T^2 attention cost and the need to store full-layer activations drive both memory bandwidth and energy cost during training.

B.2 Decoder-Only (Autoregressive)

Decoder-only (autoregressive) models (e.g. Llama3.1, GPT) perform next-token prediction and are optimized for generative tasks. The decoder processes tokens causally with a triangular mask in which each position can attend only to tokens at previous positions (and itself) to enforce autoregressive factorization. The causal mask M_{causal} has entries 0 for allowed positions and $-\infty$ for disallowed future positions, implementing the triangular attention.

Inference optimization: KV-caching. During autoregressive generation, previously computed keys and values can be cached: for step t only the new query interacts with stored $K_{1:t-1}, V_{1:t-1}$. This reduces per-step attention cost from $\mathcal{O}(t^2d)$ to $\mathcal{O}(td)$ (amortized), and reduces the energy per generated token substantially at inference time. Training a decoder-only model still incurs full-sequence $\mathcal{O}(T^2d)$ attention cost, but inference benefits from KV-caching. Energy per generated token at inference depends on cache memory bandwidth and per-layer dot-product costs; thus memory movement for KV-cache and tiled attention matmuls can dominate measured energy.

The set of activation hooks \mathcal{A}_{dec} defined similarly to the encoder case, but is adapted to handle causal inputs and cached key-value states and it stores the intermediate activations $\alpha_{\ell,t}^{\text{attn_in}}$ and $\alpha_{\ell,t}^{\text{kv}}$ for each layer ℓ and time step t . For profiling

Model	# of Layers	Hidden Dimension	Attention Heads	Feed-Forward Dimension	Parameters	Special Features
google-bert/bert-base-uncased	12	768	12	3072	110M	Uses [CLS] token for classification
google-bert/bert-large-uncased	24	1024	16	4096	340M	Larger variant of BERT with higher representational capacity
albert/albert-base-v2	12	768	12	3072	12M	Parameter-sharing across layers and factorized embedding
albert/albert-large-v2	24	1024	16	4096	18M	Deeper network with the same parameter-sharing strategy
distilbert/distilbert-base-uncased	6	768	12	3072	66M	Distilled version of BERT with 40% fewer parameters
distilroberta/distilroberta-base	6	768	12	3072	82M	Distilled version of RoBERTa retaining most performance
FacebookAI/roberta-base	12	768	12	3072	125M	Improved pretraining and dynamic masking
FacebookAI/roberta-large	24	1024	16	4096	355M	Larger RoBERTa model with improved pretraining

Table 2: Detailed architectural comparison of eight Encoder-Only models across key parameters like hidden dimension size, number of layers, number of parameters, etc.

isolated attention at generation-time, replaying using cached KV tensors models the exact inference cost. For the purpose of our analysis, we primarily consider the energy and computation associated with the generation of **a single token**, where KV-caching is not utilized

Decoder-only models are majorly different from Encoder-only models as they prioritize autoregressive causality in which causal masking changes attention sparsity and reduces parallelism during sequence generation. KV-caching and rotary/relative positional encodings are often used to support long-context amortized inference and decoder-only models commonly use tied input/output embeddings to reduce parameter counts, and favor pre-norm residual stacks for stability in deep networks. Refer Tables 4, 14, 15, 16

B.3 Encoder-Decoder

Encoder-Decoder models, also known as sequence-to-sequence (Seq2Seq) architectures, are widely used for tasks requiring input-to-output transformations such as machine translation, summarization, and code generation. Formally, given an input sequence $x = (x_1, \dots, x_{T_{\text{in}}})$, the encoder maps it to a sequence of hidden representations $H = (h_1, \dots, h_{T_{\text{in}}})$, and the decoder generates an output sequence $y = (y_1, \dots, y_{T_{\text{out}}})$ autoregressively, conditioned on H .

The encoder is a stack of L_e Transformer layers that performs contextual embedding of the input tokens. Each layer typically consists of:

- An **Attention** (Attn) mechanism that captures global dependencies within the input sequence i.e. for layer ℓ

$$\tilde{h}^{\ell-1} = \text{LN}(h^{\ell-1})$$

$$h'^{\ell} = h^{\ell-1} + \text{Attn}^{\ell}(\tilde{h}^{\ell-1})$$

$$h^{\ell} = h'^{\ell} + \text{FFN}^{\ell}(\text{LN}(h'^{\ell})).$$

- **Feedforward Network** that adds per-position nonlinear transformation to learn deeper features.

The encoder produces rich representations that capture semantic and syntactic relationships within the input sequence.

The decoder is also a stack of L_d Transformer layers, each consisting of:

- **Masked self-attention** which ensures autoregressive generation by attending only to previous positions.
- **Encoder-decoder cross-attention** mechanism to attend to the encoder hidden states H , incorporating information from the entire input sequence into each decoding step.
- A **Feedforward network** similar to the encoder.

Mathematically, for decoder layer ℓ :

$$\tilde{u}^{\ell-1} = \text{LN}(u^{\ell-1}), \quad s_{\text{self}}^{\ell} = \text{Attn}_{\text{causal}}(\tilde{u}^{\ell-1}),$$

Architecture Detail	Qwen2.5-3B-Instruct	Phi-4-Mini-Instruct	Llama-3.2-3B-Instruct	Gemma-3-4B-IT
Parameters	3.09B total (2.77B non-embedding)	4B	3.21B	4B
Layers	36	32	28	34
Hidden Size / Head Dim	2048 hidden, 128 per head	3072 hidden, 128 per head	3072 hidden, 128 per head	2560 hidden, 128 per head
Attention Structure	GQA: 16 query heads, 2 KV heads; RoPE; QKV bias; output proj. biasless	GQA: 24 query heads, 8 KV heads; Fractional RoPE (25% post-agnostic); KV cache optimized	GQA: 24 query heads, 8 KV heads; RoPE; no bias in projections	Local+Global attention mix; Q-proj: 2048-d, K/V-proj: 1024-d; q_norm, k_norm applied
MLP / FFN Dimension	SwiGLU, 11008 (up+gate), 2048 down	SiLU, 16384 (gate+up), 8192 down	SiLU, 8192 up, 3072 down	GELU-Tanh, 10240 up, 2560 down
Normalization	RMSNorm, $\epsilon = 1e-6$, applied input + post-attn	RMSNorm, $\epsilon = 1e-5$, input + post-attn	RMSNorm, $\epsilon = 1e-5$, input + post-attn	RMSNorm, $\epsilon = 1e-6$, input + post-attn + pre/post-FFN
Embeddings	151,936 vocab, 2048-d, tied in/out	200,064 vocab, 3072-d, tied in/out (padding idx=199999)	128,256 vocab, 3072-d, tied in/out	262,208 vocab, 2560-d, tied in/out, scaled embeddings
Context Length	32K tokens (gen up to 8K)	Long-context via KV optimization, tested up to $\sim 128K$	128K tokens, efficient GQA	128K tokens; local layers span 1K, 1 global layer every 5 locals
Special Features	RoPE, SwiGLU, QKV bias, high multilingual coverage	GQA w/ reduced KV cache, fractional RoPE, tuned LR schedule	Optimized transformer, SFT+RLHF alignment, multilingual	Local-global hybrid attention, multimodal (SigLIP image encoder), Pan & Scan for variable resolution

Table 3: Detailed architectural comparison of Decoder-Only Qwen2.5-3B, Phi-4-Mini, Llama-3.2-3B, and Gemma-3-4B instruction-tuned models.

$$s_{\text{cross}}^{\ell} = \text{Attn}_{\text{cross}}(\text{LN}(u^{\ell-1} + s_{\text{self}}^{\ell}), H),$$

$$u^{\ell} = \text{FFN}(\text{LN}(u^{\ell-1} + s_{\text{self}}^{\ell} + s_{\text{cross}}^{\ell})).$$

Compared to encoder-only models, the encoder-decoder architecture introduces a separate decoder stack with cross-attention, which enables output generation conditioned on the full input sequence. In contrast, encoder-only models produce fixed-length or token-level representations that are typically used for classification or embedding tasks, without any autoregressive generation.

When compared to decoder-only models, encoder-decoder architectures separate the input encoding from the output generation, whereas decoder-only models combine both within a single autoregressive stack. This separation allows the encoder to process the entire input sequence in parallel, improving training efficiency. Furthermore, in terms of residual and attention patterns, encoder-decoder models incorporate both self-attention in the decoder and cross-attention between the decoder and encoder outputs, whereas encoder-only and decoder-only architectures contain only a single attention mechanism.

Energy Perspective: The two-stack design of encoder-decoder models increases the total parameter count and memory footprint, resulting in higher energy consumption during training compared to encoder-only models for sequences of the same length. However, the input encoding phase can be fully parallelized across positions, and autoregressive decoder computation can benefit from caching mechanisms during inference, which partially reduces the per-token energy cost

B.4 Mixture of Experts (MoE)

Mixture-of-Experts (MoE) architectures extend standard Transformers by introducing conditional computation i.e. instead of activating all parameters for every input token, only a subset of "expert" networks is selected dynamically. This allows scaling model capacity substantially while keeping per-token computation and energy consumption manageable.

An MoE layer contains E independent feed-forward networks, or Experts, each with parameters $\theta_1, \dots, \theta_E$. For a given token representation

Components	Qwen2.5-3B fp32		Qwen2.5-3B fp16		Llama-3.2-3B fp32		Llama-3.2-3B fp16		Gemma-3-4B fp32		Gemma-3-4B fp16	
	Mean	Std. Dev	Mean	Std. Dev	Mean	Std. Dev	Mean	Std. Dev	Mean	Std. Dev	Mean	Std. Dev
MLP	113.71	6.687	48.5	2.13	127.24	1.94	54.55	2.01	129.47	1.86	60.07	2.13
Attention	27.64	1.79	33.99	5.96	58.31	3.01	23.88	1.42	42.82	2.11	36.84	1.85
Input Layer Norm	2.59	0.24	6.42	1.02	3.2	0.25	3.61	0.41	3.74	0.45	4.42	0.43
Attention Layer Norm	2.81	0.33	6.8	0.97	3.2	0.32	3.85	0.41	3.49	0.33	4.52	0.36
Capture (Block)	146.75	-	95.71	-	191.95	-	85.89	-	186.54	-	114.83	-
Block	150.03	3.39	96.19	5.15	192.26	24.92	91.85	1.98	187.54	3.91	126.63	4.54
%Capture (Block)	97.81		99.50		99.84		93.51		99.47		90.68	
Final Layer Norm	2.96	0.41	6.94	0.97	3.2	0.27	4.2	0.58	3.5	0.33	4.53	0.32
Embedding	0.81	0.26	0.74	0.06	0.69	0.23	0.68	0.24	1.52	0.29	1.28	0.27
LLM Head	459.66	2.18	214.29	3.56	602.02	2.97	374.92	2.96	1040.63	7.25	480.64	8.72
Model	5864.51	-	3684.81	-	5989.19	-	2951.6	-	7422.01	-	4791.87	-
Capture (Model)	5995.27	26.77	3685.95	29.11	6029.32	10.68	3261.5	30.99	8086.96	25.25	5248.99	89.34
%Capture (Model)	97.82		99.97		99.33		90.50		91.78		91.29	

Table 4: CLEAR demonstrating similar performance on RTX 5000 GPU for Decoder-only models(Qwen2.5-3B, Llama-3.2-3B, Gemma-3-4B) across fp16 and fp32 floating point precisions. The average Energy values and standard deviation values are in millijoules (mJ).

$h \in \mathbb{R}^d$, the computation is routed through a small subset of $k < E$ experts, typically $k = 2$ or 3

$$m^{\text{MoE}}(h) = \sum_{i \in \text{Top-}k} g_i(h) \text{FFN}_i(h),$$

where $g_i(h)$ is the gating weight assigned by the Router. By activating only a few experts per token, the effective FLOPs per token can be reduced from $\mathcal{O}(E \cdot d \cdot d_{\text{ff}})$ to $\mathcal{O}(k \cdot d \cdot d_{\text{ff}})$.

The Router is a lightweight module that predicts which experts should process a given token:

$$g(h) = \text{softmax}(hW_r), \quad g \in \mathbb{R}^E.$$

It selects the top- k experts according to the largest g_i values. The Router can also include auxiliary losses, such as load-balancing or importance losses, to encourage uniform expert utilization and avoid stragglers, which would increase memory or energy spikes.

By increasing the total number of experts E without increasing k , it is possible to scale the model’s representational capacity while incurring only a small incremental energy cost per token. In practice, expert computations for different tokens are often batched across devices, but load imbalance can increase memory movement and create temporary energy spikes due to which careful load-balancing and token assignment become necessary to maintain efficiency.

C Hardware Specification

The experiments in this paper were carried out using NVIDIA’s Ada-Lovelace architecture GPUs, namely the RTX 5000 Ada and RTX 6000 Ada, in order to assess compute and energy performance. The Ada Lovelace architecture is fabricated on a custom 4 nm TSMC process and includes third-generation RT cores and fourth-generation Tensor cores, enabling mixed precision operations (including FP8 with sparsity) that are integral to efficient transformer inference (NVIDIA, 2023). According to the official datasheets, the RTX 5000 Ada has 12,800 CUDA cores, 100 RT cores, 400 Tensor cores, 32 GB of ECC GDDR6 memory over a 256-bit interface (providing ~ 576 GB/s bandwidth), and a total board power of approximately 250 W (PNY, 2023). The RTX 6000 Ada model offers 18,176 CUDA cores, 142 RT cores, 568 Tensor cores, 48 GB of ECC GDDR6 memory on a 384-bit interface (~ 960 GB/s bandwidth), and has a board power of around 300 W (NVIDIA, 2023). These hardware choices directly influence both the sustained compute throughput and the energy-per-FLOP metrics reported in our results.

NVIDIA does not publish the precise NVML power sampling interval for the RTX 5000 Ada or RTX 6000 Ada. Prior work has shown that on modern NVIDIA GPUs, NVML’s power readouts are typically updated at a frequency of 20–50 Hz (i.e., every 20–50 ms), which constrains the granularity of fine-grained energy attribution (Yang et al., 2024b), (Nik et al., 2025).

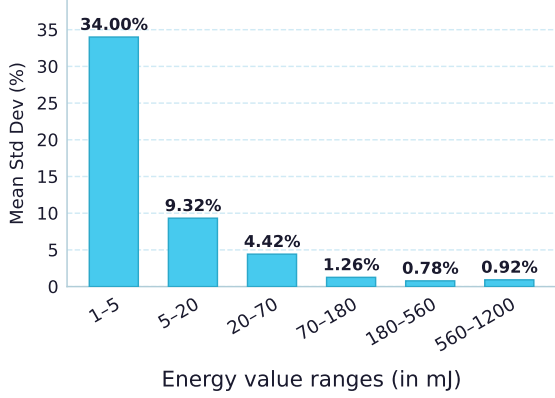


Figure 9: Standard Deviation across different Energy measurements. We observe a decrease in Standard Deviation in our Energy Measurement Approach with increasing Energy Values.

C.1 Nvidia RTX 5000 and RTX 6000

We validate our methodology across three models on the NVIDIA RTX 5000 ADA GPU and observe a %Capture exceeding 90%, with minimal standard deviation across both fp16 and fp32 precisions. Interestingly, the energy consumption of normalization blocks remains higher for fp16 compared to fp32, similar to the trend observed on the NVIDIA RTX 6000. Refer Tables 4, 14, 15, 16

D Variation in Standard Deviation

As shown in Fig. 9, the standard deviation of energy measurements exhibits a higher relative deviation at lower energy values (around 1 mJ), primarily due to the limited precision of the NVML energy sensor. For measurements above 5 mJ, the deviation stabilizes to an acceptable range of approximately 9%, and further decreases below 5% for energies exceeding 20 mJ. This behavior arises because fixed sensor resolution introduces proportionally larger errors at smaller measurement scales.

E Multi Token & KV Cache

Using CLEAR, we extend our evaluation beyond the single-token *Prefill* stage to study multi-token generation in decoder-only transformer models. Unlike single-token experiments, multi-token generation involves both the *Prefill* and *Decode* stages and introduces additional computational considerations due to Key-Value (KV) cache (Vaswani et al., 2023) optimizations.

In autoregressive decoder models, tokens are generated sequentially. For each newly generated

Input Token Length	With KV Cache			Without KV Cache		
	Avg Energy (mJ)	Std Dev.	GFLOPS	Avg Energy (mJ)	Std Dev.	GFLOPS
1	29.118	0.515	0.019	28.052	0.474	0.019
8	31.217	0.524	0.019	29.622	0.682	0.151
32	31.850	0.511	0.019	32.184	0.580	0.604
64	31.995	0.513	0.019	35.082	0.690	1.208
128	32.532	0.239	0.019	40.148	0.696	2.417
256	33.124	0.785	0.019	62.554	1.591	4.834
512	33.558	1.335	0.019	87.369	2.220	9.667

Table 5: Energy consumption and FLOP requirements for the attention mechanism in the Qwen2.5-3B model with and without KV cache across varying input sequence lengths. When KV cache is enabled, both energy usage and computational cost remain nearly constant, whereas disabling the KV cache leads to a sharp increase in FLOPs and energy as sequence length grows. The average Energy values and standard deviation values are in millijoules (mJ).

token, the attention mechanism must attend to all previously processed tokens in the sequence. In a naive implementation without caching, this requires recomputing the Key (K) and Value (V) projections for the entire sequence at every generation step. Consequently, both computational cost and energy consumption increase rapidly with sequence length due to repeated projection and attention operations.

KV caching eliminates this redundancy by storing previously computed K and V tensors during the *Prefill* stage and reusing them during subsequent *Decode* steps. During decoding, only the Query (Q) corresponding to the newly generated token needs to be computed, while all previously computed keys and values are retrieved directly from the cache. This optimization significantly reduces redundant computation and memory traffic.

Our measurements show that multi-token generation exhibits distinct scaling behavior across the *Prefill* stage, *Decode* stage, and the full generation pipeline. The *Prefill* stage processes the entire input sequence and therefore shows a near-linear increase in both FLOPs and energy consumption as the sequence length grows. This behavior arises because fresh Q , K , and V projections must be computed for every token in the sequence.

In contrast, the *Decode* stage remains nearly invariant to sequence length when KV caching is enabled. As shown in Table 5, the FLOPs remain constant at approximately 0.019 GFLOPs and the energy consumption remains nearly stable (approximately 29–33 mJ) across input lengths ranging from 1 to 512 tokens. This occurs because only

Input Token Length	Prefill		Next token Decode Stage		Output Generation	
	Avg Energy (mJ)	GFLOPs	Avg Energy (mJ)	GFLOPs	Avg Energy (mJ)	GFLOPs
1	4329.42	6.17	4472.20	6.17	4278.49	6.17
8	4531.80	49.38	4543.73	6.17	4517.82	45.02
32	4829.55	197.51	4600.39	6.17	4749.55	178.22
64	5273.63	395.03	4675.02	6.17	5254.10	355.82
128	6964.34	790.06	4749.80	6.17	6895.61	711.02
256	8959.38	1580.12	4839.23	6.17	8330.42	1421.42
512	13940.02	3160.24	5025.20	6.17	13730.38	2842.23

Table 6: Energy consumption and FLOP analysis of the Qwen2.5-3B model across varying input sequence lengths. We report measurements for three important phenomena: Prefill, Next-Token Decode (KV Cache Enabled) and Output Generation pipeline with 1 new token. The results show that while the FLOPs of the decode step remain constant due to KV reuse, its energy consumption increases only marginally with longer input lengths, in contrast to the Prefill and Output Generation where energy consumption scales rapidly with the input sequence length. The average Energy values are in millijoules (mJ).

the newly generated token is processed while all previous keys and values are reused from the cache.

When KV caching is disabled, however, the attention mechanism must recompute the entire set of Q , K , and V projections at every step. As a result, the computational cost increases rapidly with sequence length. For example, as the input sequence increases from 1 to 512 tokens, FLOPs grow from 0.019 GFLOPs to 9.667 GFLOPs, while energy consumption increases from 28.05 mJ to 87.36 mJ.

These results demonstrate that KV caching substantially reduces redundant computation in the attention mechanism and leads to significant energy savings. At longer sequence lengths, KV cache achieves energy reductions exceeding 60% compared to the uncached implementation. Figure 5 further illustrates this trend, showing both the percentage reduction in energy due to KV caching and the absolute difference in energy consumption with and without caching.

Overall, these observations highlight KV caching as a critical optimization for enabling efficient long-context autoregressive decoding. While the Prefill stage and portions of the output generation pipeline continue to scale with sequence length, KV caching ensures that the Decode stage remains computationally and energetically efficient.

F Attention Variants and Optimizations

Using **CLEAR**, we compare three Attention implementations: *Eager Attention*, *Scaled Dot-Product*

Attention (SDPA), and *Flash Attention*. Although all variants compute the same mathematical operation defined by Equation 6, they differ significantly in how the computation is scheduled and executed on GPU hardware. These differences in execution strategy lead to measurable variations in memory access patterns, kernel launch behavior, and overall energy consumption.

Energy Comparison Across Attention Variants

Across both models and all sequence lengths, Eager Attention consistently consumes the highest amount of energy. For example, in the Qwen2.5-3B model with 64 input tokens, Eager Attention consumes 45.4 mJ compared to 38.6 mJ for Flash Attention and 35.1 mJ for SDPA. A similar trend appears at larger sequence lengths: at 256 tokens, Eager Attention requires 70.4 mJ, while Flash Attention consumes 56.7 mJ and SDPA consumes 62.2 mJ.

The same behavior is observed in the Gemma3-4B model. At 64 tokens, Eager Attention consumes 67.0 mJ compared to 59.4 mJ for Flash Attention and 57.0 mJ for SDPA. At 256 tokens, Eager Attention increases to 100.2 mJ, while Flash Attention consumes 85.8 mJ and SDPA consumes 94.0 mJ.

This consistent gap in energy consumption is primarily caused by differences in memory usage and kernel execution. Eager Attention executes multiple independent GPU kernels for computing the query-key multiplication, softmax normalization, and value projection. Each of these operations launches separate GPU kernels and requires intermediate memory storage. As a result, the full attention matrix must be materialized in memory, which increases both memory traffic and kernel launch overhead.

SDPA improves upon this design by fusing some of the intermediate operations, which reduces kernel launch overhead. However, it still materializes the full attention matrix in GPU memory. Consequently, although SDPA is more efficient than Eager Attention, its memory traffic remains relatively high.

Flash Attention provides further improvements by reorganizing the computation into tiled blocks that fit into on-chip GPU memory. Instead of constructing the full attention matrix, the algorithm computes attention scores in smaller blocks and accumulates partial results. This approach significantly reduces memory movement between global memory and GPU cores. Since modern GPUs of-

Model & Input Length	Attention Setup	Energy Consumption (mJ)	Std. Deviation	FLOPs (in GFLOPs)	Energy (mJ) / GFLOP
Qwen2.5 - 3B 64 input tokens	FP16 Flash Attention	38.609	0.348	1.208	31.950
	FP16 Eager Attention	45.398	0.564	1.242	36.552
	FP16 SDPA	35.061	0.378	1.208	29.014
	FP16 Flash with torch.compile()	29.100	0.320	1.208	24.090
	FP16 Eager with torch.compile()	31.675	0.163	1.242	25.513
	BF16 Flash Attention	48.289	1.247	2.417	19.980
	FP16 Eager Max Autotune	19.679	0.664	-	-
	F16 Eager Reduce Overhead	19.640	0.765	-	-
Qwen2.5 - 3B 128 input tokens	FP16 Flash Attention	44.169	0.764	2.417	18.276
	FP16 Eager Attention	53.766	1.506	2.551	21.074
	FP16 SDPA	39.577	0.642	2.417	16.376
	FP16 Flash with torch.compile()	33.337	0.441	2.416	13.799
	FP16 Eager with torch.compile()	38.881	0.947	2.550	15.247
	BF16 Flash Attention	48.289	1.247	2.417	19.980
	FP16 Eager Max Autotune	24.977	0.318	-	-
	F16 Eager Reduce Overhead	24.233	0.881	-	-
Qwen2.5 - 3B 256 input tokens	FP16 Flash Attention	56.665	1.131	4.834	11.723
	FP16 Eager Attention	70.411	0.585	5.372	13.108
	FP16 SDPA	62.223	1.319	4.834	12.873
	FP16 Flash with torch.compile()	47.558	0.702	4.832	9.843
	FP16 Eager with torch.compile()	59.949	0.818	5.369	11.166
	BF16 Flash Attention	48.289	1.247	2.417	19.980
	FP16 Eager Max Autotune	33.500	0.874	-	-
	F16 Eager Reduce Overhead	36.626	1.095	-	-
Gemma3 - 4B 64 input tokens	FP16 Flash Attention	59.416	0.882	2.014	29.498
	FP16 Eager Attention	66.962	0.694	2.048	32.699
	FP16 SDPA	57.048	1.035	2.014	28.322
	FP16 Flash with torch.compile()	32.953	0.461	2.013	16.368
	FP16 Eager with torch.compile()	34.322	0.383	2.047	16.769
	BF16 Flash Attention	67.633	0.986	2.014	33.577
	FP16 Eager Max Autotune	23.842	0.762	-	-
	F16 Eager Reduce Overhead	23.827	0.841	-	-
Gemma3 - 4B 128 input tokens	FP16 Flash Attention	69.228	0.749	4.029	17.184
	FP16 Eager Attention	76.126	0.658	4.163	18.287
	FP16 SDPA	65.785	0.504	4.029	16.330
	FP16 Flash with torch.compile()	43.885	0.558	4.027	10.899
	FP16 Eager with torch.compile()	44.267	0.562	4.161	10.639
	BF16 Flash Attention	76.328	1.326	4.029	18.947
	FP16 Eager Max Autotune	30.591	0.852	-	-
	F16 Eager Reduce Overhead	31.651	0.851	-	-
Gemma3 - 4B 256 input tokens	FP16 Flash Attention	85.843	1.854	8.057	10.654
	FP16 Eager Attention	100.152	2.179	8.594	11.653
	FP16 SDPA	93.987	1.188	8.057	11.665
	FP16 Flash with torch.compile()	58.833	0.814	8.053	7.306
	FP16 Eager with torch.compile()	60.907	0.696	8.590	7.091
	BF16 Flash Attention	101.571	3.304	8.057	12.607
	FP16 Eager Max Autotune	41.614	0.619	-	-
	F16 Eager Reduce Overhead	44.674	0.161	-	-

Table 7: Average Energy Consumption, FLOPs and Energy(mJ)/GFLOPs ratio for Gemma3-4B and Qwen2.5-3B models across input token lengths of 64, 128 and 256. We demonstrate results for 3 Attention Variants (SDPA, Eager, Flash) along with Optimizations such as Torch Compile, Max Autotune and Reduced Overhead. The average Energy values and standard deviation values are in millijoules (mJ).

ten spend more energy on memory access than on arithmetic computation, reducing memory traffic leads to lower overall energy consumption.

Impact of Sequence Length on Energy Efficiency

Table 7 also shows that total energy consumption increases as sequence length grows, but the *energy per GFLOP* decreases. For example, in the Qwen2.5-3B model using Flash Attention, total energy increases from 38.6 mJ at 64 tokens to 56.7 mJ at 256 tokens. However, the energy per GFLOP decreases from 31.95 mJ/GFLOP to 11.72 mJ/GFLOP.

A similar trend can be observed in the Gemma3-4B model. Flash Attention consumes 59.4 mJ at 64 tokens and 85.8 mJ at 256 tokens, while the energy per GFLOP decreases from 29.50 mJ/GFLOP to 10.65 mJ/GFLOP.

The behavior can be explained by the energy modelling as a function of FLOPs described in Equation 5. The total energy consumed by a component includes a fixed overhead term E_0 and a variable compute-dependent term. The fixed component includes kernel launch overhead, memory allocation, and GPU setup costs. When the sequence length is small, the fixed cost represents a large fraction of the total energy. As the sequence length increases, the computation grows faster than the fixed overhead, causing the energy cost to amortize across more operations. As a result, the energy consumed per unit of computation (mJ/GFLOP) decreases.

Effect of Torch Compile

We isolate the effect of `torch.compile()`, which performs graph-level optimization and kernel fusion. Across both models, `torch.compile()` significantly reduces energy consumption for both Flash and Eager Attention.

For example, in Qwen2.5-3B with 256 tokens, Flash Attention consumes 56.7 mJ in the baseline implementation but only 47.6 mJ when `torch.compile` is enabled. Similarly, Eager Attention decreases from 70.4 mJ to 59.9 mJ after compilation. In the Gemma3-4B model at 256 tokens, Flash Attention drops from 85.8 mJ to 58.8 mJ, while Eager Attention drops from 100.2 mJ to 60.9 mJ.

The improvement occurs because `torch.compile()` analyzes the execution graph and merges multiple small GPU kernels into fewer,

larger kernels. Larger kernels reduce kernel launch overhead and allow the GPU to maintain higher utilization. Kernel fusion also eliminates many intermediate memory reads and writes, which reduces memory traffic and therefore lowers energy consumption.

Effect of Precision

The results also show that BF16 precision slightly increases energy consumption compared to FP16. For example, in Qwen2.5-3B with 64 tokens, BF16 Flash Attention consumes 48.3 mJ compared to 38.6 mJ for FP16 Flash Attention. In Gemma3-4B with 256 tokens, BF16 Flash Attention consumes 101.6 mJ compared to 85.8 mJ for FP16 Flash Attention.

This difference arises because some GPU architectures internally convert BF16 operations to FP32 during execution. These conversion steps introduce additional arithmetic operations and memory movement, which slightly increases the total energy consumed.

Aggressive Kernel Optimization

The most significant reduction in energy consumption occurs with the **Max Autotune** and **Reduced Overhead** optimization modes. These configurations produce the lowest energy values across all models and sequence lengths.

For example, in Qwen2.5-3B with 256 tokens, Max Autotune reduces energy consumption to 33.5 mJ and Reduced Overhead reduces it to 36.6 mJ. Similarly, in Gemma3-4B with 256 tokens, energy decreases to 41.6 mJ with Max Autotune and 44.7 mJ with Reduced Overhead. These values are significantly lower than the baseline implementations.

These optimizations work by aggressively fusing operations and selecting hardware-specific kernel implementations. Max Autotune performs extensive kernel benchmarking during compilation to determine the most efficient kernel configurations for the current hardware. This includes searching over tile sizes, block sizes, memory layouts, and execution schedules. Reduced Overhead removes profiling and synchronization steps that are typically inserted during model execution, which further reduces kernel launch overhead.

Limitations of FLOP Measurement

For the Max Autotune and Reduced Overhead configurations, it is not possible to reliably measure

FLOPs using standard profiling tools. These optimizations generate fused kernels that combine multiple operations such as matrix multiplication, softmax normalization, and scaling into a single hardware-level kernel. Because these fused kernels no longer correspond to individual high-level operators, existing profiling tools cannot accurately attribute a FLOP count to each operation. As a result, the FLOP values for these configurations are not reported in Table 7.

G Additional Results

Components	ALBERT		BERT		DistilBERT		RoBERTa	
	Avg.	Std. Dev	Avg.	Std. Dev	Avg.	Std. Dev	Avg.	Std. Dev
Attention Block	12.074	0.280	13.676	0.370	10.550	0.369	13.534	0.319
FFN (Intermediate)	1.510	0.441	2.765	0.192	8.764	0.442	2.565	0.321
FFN (Output)	1.848	0.050	4.944	0.343			4.875	0.401
Norm. (All)	7.317	0.531	6.216	0.845	7.135	0.369	6.352	0.623
Captured (Block)	22.748	-	27.601	-	26.449	-	27.326	-
Measured (Block)	30.627	0.562	29.802	0.607	28.551	0.448	29.797	0.642
%Capture (Block)	74.276	-	92.616	-	92.637	-	91.707	-
# of Layers	12	-	12	-	6	-	12	-
Embedding Layer	5.863	0.328	5.918	0.307	4.619	0.161	11.911	0.159
CLS + LM Head	11.687	0.455	23.666	0.979	18.396	1.009	41.081	0.907
Captured (Model)	385.068	-	387.205	-	194.320	-	410.555	-
Total	424.039	6.548	400.449	4.805	209.734	5.053	413.318	5.943
%Capture (Model)	90.810	-	96.693	-	92.651	-	99.332	-

Table 8: Comparison of FP16 Performance across ALBERT, BERT, DistilBERT, RoBERTa. The average Energy values and standard deviation values are in millijoules (mJ).

Components	ALBERT - Large		BERT - Large		Distil RoBERTa		RoBERTa - Large	
	Avg.	Std. Dev	Avg.	Std. Dev	Avg.	Std. Dev	Avg.	Std. Dev
Attention Block	14.861	0.423	16.903	0.397	13.226	0.349	15.547	0.370
FFN (Intermediate)	2.928	0.743	4.877	0.456	7.413	0.396	4.249	0.115
FFN (Output)	3.939	0.710	8.093	0.462			7.741	0.443
Norm. (All)	5.814	0.652	4.171	0.872	4.274	0.711	4.721	0.671
Captured (Block)	27.542	-	34.044	-	24.913	-	32.259	-
Block	34.293	0.493	34.590	0.709	28.670	0.511	33.854	0.833
%Capture (Block)	80.314	-	98.419	-	86.896	-	95.287	-
# of Layers	24	-	24	-	6	-	24	-
Embedding Layer	6.132	0.341	7.035	0.405	11.699	0.454	12.055	0.337
CLS + LM Head	12.142	0.671	30.928	0.831	39.096	0.908	52.381	0.721
Captured (Model)	841.313	-	868.134	-	222.813	-	876.937	-
Total	919.899	16.661	855.146	17.813	235.813	3.939	870.188	4.681
%Capture (Model)	91.457	-	101.519	-	94.487	-	100.776	-

Table 9: Comparison of FP16 Performance across variants- ALBERT Large, BERT Large, DistilRoBERTa, RoBERTa Large. The average Energy values and standard deviation values are in millijoules (mJ).

Components	ALBERT		BERT		DistilBERT		RoBERTa	
	Avg.	Std. Dev	Avg.	Std. Dev	Avg.	Std. Dev	Avg.	Std. Dev
Attention Block	18.573	0.517	19.155	0.436	17.772	0.412	17.870	0.327
FFN (Intermediate)	4.969	0.980	7.163	0.880	17.486	0.774	6.446	0.724
FFN (Output)	5.066	0.935	9.528	0.646			8.829	0.620
Norm. (All)	5.267	0.432	4.023	0.972	5.872	0.861	4.721	0.671
Captured (Block)	33.875	-	39.869	-	41.130	-	37.867	-
Block	40.282	0.779	42.030	0.881	46.199	0.755	40.054	1.545
%Capture (Block)	84.095	-	94.858	-	89.028	-	94.540	-
# of Layers	12	-	12	-	6	-	12	-
Embedding Layer	6.326	0.362	6.395	0.304	4.317	0.398	11.463	0.213
CLS + LM Head	20.468	0.455	48.188	0.979	39.096	0.908	74.482	1.008
Captured (Model)	510.181	-	558.945	-	320.608	-	566.588	-
Total	562.878	9.828	595.044	9.741	350.642	6.380	638.949	13.632
%Capture (Model)	90.638	-	93.933	-	91.435	-	88.675	-

Table 10: Comparison of FP32 Performance across ALBERT, BERT, DistilBERT, RoBERTa. The average Energy values and standard deviation values are in millijoules (mJ).

Components	ALBERT - Large		BERT - Large		Distil RoBERTa		RoBERTa - Large	
	Avg.	Std. Dev	Avg.	Std. Dev	Avg.	Std. Dev	Avg.	Std. Dev
Attention Block	23.380	0.545	25.777	0.546	19.888	0.493	24.569	0.572
FFN (Intermediate)	8.139	1.049	9.679	0.929	7.275	0.924	9.145	0.949
FFN (Output)	8.090	0.843	12.952	0.799	9.636	0.679	12.124	0.817
Norm. (All)	4.479	0.512	4.413	0.872	3.761	0.843	4.310	0.871
Captured (Block)	44.089	-	52.821	-	40.561	-	50.148	-
Block	60.662	0.918	58.006	0.841	42.234	1.687	55.608	1.023
%Capture (Block)	72.680	-	91.061	-	96.038	-	90.183	-
# of Layers	24	-	24.000	-	6.000	-	24.000	-
Embedding Layer	5.910	0.345	7.080	0.401	14.044	0.541	13.559	0.363
CLS + LM Head	20.003	0.500	62.534	1.021	75.561	0.936	97.300	0.746
Captured (Model)	1481.807	-	1461.768	-	343.009	-	1445.440	-
Total	1562.929	9.036	1485.891	13.015	350.642	6.380	1484.479	11.134
%Capture (Model)	94.810	-	98.376	-	97.823	-	97.370	-

Table 11: Comparison of FP32 Performance across large variants of ALBERT, BERT, DistilBERT, RoBERTa. The average Energy values and standard deviation values are in millijoules (mJ).

Component	32 Tokens		64 Tokens		96 Tokens		128 Tokens	
	Avg.	Std. Dev.	Avg.	Std. Dev.	Avg.	Std. Dev.	Avg.	Std. Dev.
ALBERT-Base								
Attention Block	15.094	0.404	15.930	0.354	18.582	0.319	19.861	0.468
FFN (Intermediate)	2.306	0.448	2.205	0.475	3.341	0.308	3.650	0.594
FFN (Output)	2.361	0.423	2.891	0.599	4.608	0.837	4.162	0.751
Block	35.079	0.368	37.240	0.231	44.233	0.837	45.274	0.835
Embedding Layer	6.810	0.354	6.883	0.321	7.767	0.389	6.981	0.337
CLS + LM Head	13.384	0.691	14.438	0.564	17.171	0.588	19.246	0.888
Captured (Model)	441.146	-	468.198	-	555.734	-	569.510	-
Model	482.402	9.206	505.909	4.497	571.390	2.964	598.701	5.728
% Capture (Model)	91.448	-	92.546	-	97.260	-	95.124	-
BERT- Base								
Attention Block	15.337	0.398	17.988	0.466	18.949	0.237	19.518	0.358
FFN (Intermediate)	3.472	0.393	3.695	0.186	4.628	0.494	5.626	0.653
FFN (Output)	5.210	0.374	5.947	0.361	7.450	0.290	8.774	0.272
Block	32.585	0.487	34.980	0.871	39.130	0.938	41.482	1.039
Embedding Layer	6.938	0.304	8.004	0.401	7.812	0.378	7.553	0.046
CLS + LM Head	24.876	0.906	31.174	0.798	31.497	0.615	39.772	0.897
Captured (Model)	422.840	-	458.936	-	508.874	-	545.111	-
Model	450.756	4.650	465.372	2.665	523.566	8.469	557.446	6.968
% Capture (Model)	93.807	-	98.617	-	97.194	-	97.787	-
DistilBERT								
Attention Block	12.501	0.480	13.708	0.399	14.593	0.437	14.524	0.402
FFN	10.489	0.414	10.365	0.298	13.227	0.649	14.665	0.536
Block	32.794	0.791	34.432	0.775	38.200	1.049	39.894	0.579
Embedding Layer	5.322	0.258	5.503	0.352	5.583	0.276	5.043	0.137
CLS + LM Head	20.512	0.486	27.341	0.877	26.021	0.798	34.210	0.841
Captured (Model)	222.597	-	239.438	-	260.806	-	278.618	-
Model	234.498	4.466	245.985	4.135	279.116	4.422	304.458	5.907
% Capture (Model)	94.925	-	97.338	-	93.440	-	91.513	-
RoBERTa								
Attention Block	14.996	0.398	17.547	0.438	18.979	0.426	18.479	0.332
FFN (Intermediate)	3.368	0.412	3.418	0.170	4.657	0.496	5.582	0.655
FFN (Output)	5.204	0.349	5.687	0.396	7.378	0.196	8.331	0.526
Block	32.960	0.703	35.684	1.005	40.294	1.569	41.712	1.503
Embedding Layer	12.383	0.360	14.455	0.541	15.189	0.778	12.794	0.345
CLS + LM Head	39.649	0.872	55.586	0.626	70.320	0.797	77.164	1.159
Captured (Model)	447.552	-	498.249	-	545.035	-	590.506	-
Model	470.720	5.510	506.925	5.836	553.857	4.894	594.927	7.070
% Capture (Model)	95.078	-	98.289	-	98.407	-	99.257	-

Table 12: Energy consumption trends with varying input token lengths (tokens) for encoder only (Base) models. The average Energy values and standard deviation values are in millijoules (mJ).

Component	32 Tokens		64 Tokens		96 Tokens		128 Tokens	
	Avg.	Std. Dev.	Avg.	Std. Dev.	Avg.	Std. Dev.	Avg.	Std. Dev.
ALBERT-Large								
Attention Block	17.730	0.472	19.696	0.645	22.541	0.529	24.279	0.435
FFN (Intermediate)	3.364	0.812	3.399	0.927	5.134	0.888	4.352	0.821
FFN (Output)	4.117	0.688	4.724	0.900	5.424	0.956	6.064	0.913
Block	39.912	0.474	44.930	1.058	51.089	0.969	55.649	0.597
Embedding Layer	7.881	0.163	7.846	0.417	7.849	0.397	7.914	0.383
CLS + LM Head	14.461	0.671	15.293	0.715	17.528	0.609	22.213	0.457
Captured (Model)	980.23	-	1101.46	-	1251.52	-	1365.71	-
Model	1029.60	5.731	1151.70	20.540	1320.18	9.018	1394.97	7.538
% Capture (Model)	95.205	-	95.638	-	94.799	-	97.903	-
BERT- Large								
Attention Block	18.641	0.275	20.986	0.405	23.092	0.670	24.792	0.351
FFN (Intermediate)	5.424	0.208	6.216	0.630	7.962	0.797	7.189	0.766
FFN (Output)	8.593	0.491	9.499	0.541	12.091	0.859	12.533	0.752
Block	37.557	0.942	41.864	1.259	48.511	1.519	50.453	1.124
Embedding Layer	7.729	0.311	8.106	0.413	8.131	0.403	8.145	0.326
CLS + LM Head	32.645	0.943	39.421	0.926	41.166	0.892	40.203	0.470
Captured (Model)	941.732	-	1052.26	-	1213.56	-	1259.22	-
Model	932.191	13.932	1060.72	28.963	1206.09	13.967	1276.73	8.691
% Capture (Model)	101.024	-	99.202	-	100.620	-	98.628	-
Distil RoBERTa								
Attention Block	15.753	0.276	17.618	0.401	18.913	0.426	18.517	0.365
FFN	3.499	0.374	3.542	0.343	4.595	0.508	5.488	0.679
Block	5.287	0.354	5.664	0.450	7.623	0.423	8.228	0.474
Embedding Layer	33.617	0.759	35.723	1.081	39.958	1.678	41.404	1.463
CLS + LM Head	12.882	0.307	14.689	0.416	14.714	0.358	12.636	0.346
Captured (Model)	39.648	0.854	55.718	0.776	70.263	0.816	77.483	1.026
Model	254.234	-	284.747	-	324.726	-	338.543	-
% Capture (Model)	270.513	4.867	292.914	3.888	319.139	5.044	341.740	5.520
RoBERTa-Large								
Attention Block	18.648	0.346	20.390	0.353	22.573	0.386	24.780	0.474
FFN (Intermediate)	5.437	0.219	5.567	0.131	7.809	0.834	7.066	0.813
FFN (Output)	8.476	0.553	9.417	0.539	11.755	0.691	12.475	0.750
Block	36.273	0.979	40.831	1.651	47.154	1.870	50.343	1.970
Embedding Layer	14.251	0.372	14.534	0.406	14.647	0.411	14.609	0.391
CLS + LM Head	51.022	0.958	69.201	1.015	89.032	1.128	94.427	0.949
Captured (Model)	935.819	-	1063.67	-	1235.36	-	1317.27	-
Model	965.216	9.228	1054.90	6.207	1238.24	10.077	1347.08	23.636
% Capture (Model)	96.954	-	100.831	-	99.768	-	97.787	-

Table 13: Energy consumption trends with varying input token lengths (tokens) for encoder only (Large) models. The average Energy values and standard deviation values are in millijoules (mJ).

Component	32 Tokens		64 Tokens		96 Tokens		128 Tokens	
	Avg.	Std. Dev.	Avg.	Std. Dev.	Avg.	Std. Dev.	Avg.	Std. Dev.
Gemma-3 4B								
Attention Block	47.312	1.421	53.619	1.672	64.300	1.381	65.488	1.050
MLP	73.218	1.043	75.700	0.872	81.383	0.776	83.230	0.995
Norm. (All)	26.144	0.533	27.853	0.456	30.892	0.394	32.878	0.877
Captured (Block)	146.674	-	157.173	-	176.575	-	181.596	-
Block	152.390	2.879	166.800	3.389	191.299	3.063	197.011	3.642
% Capture (Block)	96.249	-	94.229	-	92.303	-	92.176	-
Embedding Layer	1.916	0.399	2.078	0.430	2.147	0.451	2.258	0.454
LM Head	524.027	1.673	533.766	1.431	558.508	1.785	570.688	1.820
Final Layer Norm.	6.318	0.348	6.644	0.419	7.399	0.394	7.871	0.284
Captured (Model)	5713.511	-	6213.671	-	7072.219	-	7279.177	-
Model	6208.532	116.391	6752.334	88.871	7803.634	114.325	8047.096	104.472
% Capture (Model)	92.027	-	92.023	-	90.627	-	90.457	-
Qwen2.5 3B								
Attention Block	29.281	1.056	32.595	1.417	58.270	1.295	67.588	1.540
MLP	68.649	1.394	71.329	1.926	163.531	0.565	167.899	0.807
Norm	10.560	2.141	11.796	1.939	21.905	2.161	22.756	2.172
Captured (Block)	108.490	-	115.721	-	243.706	-	258.242	-
Block	113.174	1.417	126.411	2.573	246.125	5.963	260.012	3.274
% Capture (Block)	95.861	-	91.543	-	99.017	-	99.319	-
Embedding Layer	1.047	0.407	2.514	0.937	2.648	1.108	2.794	1.014
LM Head	243.657	3.644	250.085	0.974	530.914	2.714	544.742	2.560
Final Layer Norm	5.149	1.057	5.451	0.426	10.769	1.012	11.206	1.117
Captured (Model)	4324.124	-	4808.860	-	9404.846	-	9919.159	-
Model	4772.004	105.363	5345.951	133.036	10322.788	66.151	10727.263	84.912
% Capture (Model)	90.614	-	89.953	-	91.108	-	92.467	-
Phi3 4B								
Attention Block	67.834	1.684	72.138	1.266	81.806	1.367	89.256	1.127
MLP	134.556	1.434	148.118	1.147	155.105	1.371	168.813	0.799
Norm	20.899	2.071	21.425	2.088	22.952	2.187	23.385	2.118
Captured (Block)	223.289	-	241.681	-	259.864	-	281.453	-
Block	229.321	1.148	264.038	1.582	281.425	2.429	298.016	2.439
% Capture (Block)	97.370	-	91.533	-	92.338	-	94.442	-
Embedding Layer	2.773	1.058	2.731	1.043	2.769	1.089	2.948	1.142
LM Head	957.378	4.961	995.880	13.324	1057.904	12.474	1073.472	13.378
Final Layer Norm	10.237	0.979	10.525	1.048	11.284	1.109	11.640	1.096
Captured (Model)	8308.650	-	9458.356	-	10077.566	-	10624.575	-
Model	9204.600	57.325	10331.063	92.475	11397.891	93.548	11833.962	135.785
% Capture (Model)	90.266	-	91.553	-	88.416	-	89.780	-
Llama3.2-3B								
Attention Block	45.932	0.763	54.380	0.706	61.239	0.839	66.667	0.868
MLP	71.231	0.909	73.539	1.012	81.115	0.827	83.050	0.827
Norm	11.340	1.014	13.562	0.886	14.683	1.140	15.614	1.178
Captured (Block)	128.503	-	141.480	-	157.038	-	165.331	-
Block	130.671	2.226	150.432	2.536	157.551	1.014	167.592	1.002
% Capture (Block)	98.341	-	94.049	-	99.674	-	98.651	-
Embedding Layer	1.070	0.420	1.177	0.439	1.090	0.412	1.109	0.424
LM Head	307.571	0.948	314.289	0.958	322.029	0.685	328.267	1.114
Final Layer Norm	5.327	0.471	6.259	0.435	6.993	0.510	6.993	0.510
Captured (Model)	3972.744	-	4533.818	-	4741.546	-	5028.947	-
Model	4295.739	80.010	4966.015	94.550	5156.262	8.688	5148.606	11.498
% Capture (Model)	92.481	-	91.297	-	91.957	-	97.676	-

Table 14: Energy of Decoder Model Components using CLEAR on RTX 6000 GPU for models(Qwen2.5-3B, Llama-3.2-3B, Gemma-3-4B, Phi3-4B) with fp16 across token length. The average Energy values and standard deviation values are in millijoules (mJ).

Components	Qwen2.5		Llama3.2		Gemma 3		Phi-3 4B	
	Avg.	Std. Dev.	Avg.	Std. Dev.	Avg.	Std. Dev.	Avg.	Std. Dev.
Attention Block	32.791	1.090	42.842	0.427	45.215	0.632	62.817	0.831
MLP	62.257	1.130	64.830	1.774	66.196	1.642	132.590	2.548
Norm. (All)	9.769	0.812	9.801	0.845	23.643	1.117	20.437	1.940
Captured (Block)	104.818	-	117.473	-	135.054	-	215.843	-
Block	113.095	1.855	121.860	2.067	149.414	3.911	214.413	1.106
%Capture(Block)	92.682	-	96.400	-	90.389	-	100.667	-
Final Layer norm	4.717	0.386	4.640	0.392	5.712	0.259	10.066	0.886
Embedding Layer	0.652	0.246	0.699	0.241	1.526	0.294	1.733	0.605
LM Head	238.235	0.911	301.543	1.161	514.961	1.677	909.761	3.865
Captured Model	4315.021	-	3718.967	-	5602.269	-	9069.265	-
Model	4489.638	24.041	3996.546	81.766	5941.196	72.389	8945.062	37.252
%Capture (Model)	96.111	-	93.055	-	94.295	-	101.389	-

Table 15: Energy of Decoder Model Components using CLEAR on RTX 6000 GPU for models(Qwen2.5-3B, Llama-3.2-3B, Gemma-3-4B, Phi3-4B) with fp16 and 8 token length. The average Energy values and standard deviation values are in millijoules (mJ).

Components	Qwen2.5		Llama		Gemma		Phi	
	Avg.	Std. Dev.	Avg.	Std. Dev.	Avg.	Std. Dev.	Avg.	Std. Dev.
Attention Block	49.584	0.891	90.613	0.930	83.220	1.302	88.889	0.893
MLP	132.007	1.069	149.203	1.259	144.130	0.776	143.361	0.984
Norm. (All)	7.068	0.206	7.310	0.228	16.947	1.480	7.736	0.220
Captured (Block)	188.659	-	247.125	-	244.297	-	239.986	-
Block	187.446	1.181	241.463	0.959	257.972	6.467	249.932	6.578
%Capture (Block)	100.647	-	102.345	-	94.699	-	96.020	-
Final Layer norm	3.358	0.013	3.454	0.071	4.021	0.323	3.604	0.076
Embedding Layer	0.672	0.256	0.849	0.034	1.774	0.046	1.259	0.549
CLS + LM Head	493.335	0.977	641.738	2.972	1112.893	13.443	1159.335	14.785
Captured Model	7245.422	-	7407.010	-	9889.742	-	9162.032	-
Model	7538.858	4.374	7724.147	20.110	10685.492	28.237	9605.711	30.790
%Capture (Model)	96.108	-	95.894	-	92.553	-	95.381	-

Table 16: Energy of Decoder Model Components using CLEAR on RTX 6000 GPU for models(Qwen2.5-3B, Llama-3.2-3B, Gemma-3-4B, Phi3-4B) with fp32 and 8 token length. The average Energy values and standard deviation values are in millijoules (mJ).